



**Politecnico
di Torino**

Master's Degree in Mathematical Engineering
Mathematical Modeling and Numerical Simulation

Master's Degree Thesis

**ROLE OF THE NETWORK STRUCTURE
IN DISPERSION PROCESSES
IN BRAIDED RIVERS**

Supervisors

Prof. Carlo Vincenzo CAMPOREALE

Prof. Luca RIDOLFI

Candidate

Margherita VENDRUSCOLO

July 2023

Abstract

Braided rivers are a fluvial class characterized by the presence of multiple channels with different sizes and hydrological properties. The channels diverge and intersect continuously thus forming an extremely complex network. When a substance (like a chemical, a nutrient or a pollutant) is introduced in the watercourse, it undergoes a mixing effect which can be partly attributed to the river geomorphology, i.e. the properties of the network. This phenomenon manifests itself in a spread of travel time distributions at the outlet and is known as geomorphological dispersion.

In our thesis work we develop a mathematical model for this dispersion process. Starting from the original geomorphological instantaneous unit hydrograph (GIUH) theory, we adjust the hypothesis to apply it to the case of braided rivers and obtain a closed form to compute outlet discharges with a dependency on geomorphology. Then we perform numerical simulations on small networks aimed at validating the model and pointing out the most interesting features of the theory. Our results suggest that the network structure plays a predominant role over the branches length or the probability values associated with them, indicating that this phenomenon is mainly determined at the scale of the entire network rather than the scale of the individual channel.

Table of Contents

Introduction	1
1 Physical aspects	4
1.1 Transport processes in river networks	4
1.2 Effect of the network on dispersion	7
1.3 Braided rivers	9
1.4 Rivers and graph theory	12
2 Mathematical model	14
2.1 Review of Geomorphological Dispersion	14
2.1.1 Rodriguez-Iturbe's approach	14
2.1.2 Gupta's approach	18
2.2 Further studies	20
2.3 Residence Time Distributions	21
2.4 Model	22
3 Results	26
3.1 Toy networks	26
3.2 The Borbera network	29
3.2.1 Site description	29
3.2.2 Graph description	29
3.3 Simulations on a single-inlet single-outlet network	31
3.3.1 Network description	31
3.3.2 Equal waiting times and symmetric bifurcations	32
3.3.3 Enhanced network	33
3.3.4 Multiple waiting times	34
3.3.5 Non-symmetric bifurcations	36
3.3.6 IUH dependency on time and bifurcation values.	36
3.4 Simulations on a multiple-inlet multiple-outlet network	39
3.4.1 Network description	39
3.4.2 Equal waiting times and symmetric bifurcations	40

3.4.3 Non-symmetric bifurcations	41
Conclusions	45
Bibliography	47

Introduction

Imagine to stand on a bridge over a river channel and to throw some leaves all together into the water underneath. You will notice that all of them immediately start flowing downstream, transported by the current; at the same time though each leaf will be subject to different chaotic motions, along the other directions (depth and width) of the channel. If someone else is waiting at an outlet point, further down along the channel, they will not see the leaves arriving all together, but rather at different times and at different locations in the width of the river.

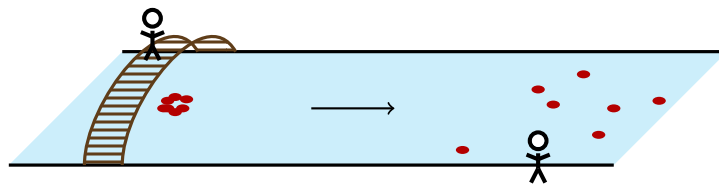


Figure 1: Sketch representing the effects of transport processes in a river, as described in the introductory example. The leaves thrown in a channel are not only carried downstream by the current, they also spread out in the other directions due to the different transport mechanisms in action.

The behaviour of the leaves, following different trajectories in their travel along the channel and spreading out in all directions, is the consequence of various *transport processes* that are simultaneously in action during water flow. Studying these phenomena is extremely important in order to trace the presence in natural rivers of substances which can significantly impact the surrounding environment, for example the release of pollutants, the distribution of nutrients. . .

More specifically we may be interested in quantifying the time it takes for a substance particle starting at an injection point in the river to reach a downstream outlet. This is known as *travel time*; it can give us an idea of response discharge of the river network to different input forcings, which are usually in the form of rainfall. If instead we want to compute the storage capacity of the catchment, meaning how long particles can stay within a certain control volume, depending on

their injection time but regardless of the exit time, then we deal with *residence time* distributions. These two concepts are usually different, but they are certainly linked (Botter, Bertuzzo, et al. 2011; Rigon, Bancheri, and Green 2016).

The most important transport processes in fluvial networks are *advection*, that is the downstream transport due to current, which we easily observe, and *dispersion*, that is responsible for the spread in travel time distributions and the chaotic motions of the leaves in the example above. The term dispersion actually reunites several mechanisms which all have the same spreading effect, but are to be ascribed to different reasons (Runkel and Bencala 1995). Physically it is virtually impossible to separate the processes and observe them individually, but this can be done with a mathematical approach, in order to understand which mechanisms give larger contributions and under which conditions.

Our work focuses specifically on the theory of *geomorphological dispersion*, a spread in travel times that is caused by the river network geometry exclusively. Rodriguez-Iturbe and Valdés introduced for the first time in 1979 the theory of geomorphological instantaneous unit hydrograph (GIUH) relating the discharge at the outlet to the river geometric properties. Indeed just the complexity of a network, with bifurcations and confluences, with branches of different lengths, acts as a natural ‘mixer’ of particles and results in a wider distribution of travel times. This occurs because the water particles have a multitude of possible paths to follow, each with its own length, and the path choice results in a different travel time through the network. Several mathematical models have been proposed to study this matter (Gupta et al. 1980; Rinaldo, Marani, et al. 1991) over the years. We have adopted the original theory of Rodriguez-Iturbe and Valdés (1979), but have removed their simplifying assumptions about the geometry, in order to apply the model to a very specific and interesting case.

Namely, for our purposes the study of geomorphological dispersion has been addressed to *braided rivers* in particular. This term indicates a class of fluvial networks known for their fascinating morphology, composed of multiple channels of different sizes, that bifurcate and intersect at various points, forming bars between channels (an example is shown in figure 2). Braided rivers are also characterized by a very dynamic behaviour because sediments transported by the current can easily obstruct some channels, deactivating them, and form new ones, so the number and the distribution of active channels is in constant evolution. We have made the choice of restricting ourselves to this category of rivers for two reasons; firstly countless investigations have been conducted as regards to braided river morphodynamics, but not as many in terms of mass and chemicals transport. Furthermore we expect geomorphological dispersion to play a predominant role in the spread of travel times in such naturally complex networks.

This thesis is organised as follows. In the first chapter the theme is presented



Figure 2: Picture of the River Tagliamento in Friuli Venezia Giulia. An example of Italian braided river, famous for being one of the few large rivers in Europe whose morphology has not been altered by artificial intervention. Photo credit: www.udine20.it.

from a physical-engineering point of view. Water transport processes in fluvial networks are described in depth and a special emphasis is put on dispersion mechanisms. A section is dedicated to investigating the dispersive role of network geometry, pointing out that it manifests itself not only in rivers but in other types of networks as well. Afterwards some qualitative notion on braided rivers is given, in order to address the object of our study.

The second chapter is devoted the mathematical model. We start with a review of the most significant steps in geomorphological dispersion theory, accurately presenting the most important approaches (Rodriguez-Iturbe and Valdés 1979; Gupta et al. 1980) and more swiftly the following advancements. Then we further develop Rodriguez-Iturbe and Valdés’ model consistently with our purposes, justifying the choices made for this thesis work.

In the third and last chapter we show the results of the simulations, obtained through the MATLAB implementation of the mathematical model. We perform tests on simple networks aimed at illustrating the key factors that influence travel time dispersion in braided rivers. Together with the network structure itself, we investigate the effect of some network properties such as the branches waiting time and the volume distribution at bifurcations.

Chapter 1

Physical aspects

1.1 Transport processes in river networks

As already mentioned, in rivers and streams the motion of water and the substances dissolved in it is the result of many different physical processes. The necessity of studying solutes transport can be easily explained through environmental and biological reasons. For example those substances might be pollutants (like hydrocarbons, pesticides. . .) that penetrate in a watercourse and need to be traced because they constitute a threat; or they could be natural substances such as nutrients, whose presence determines the evolution of biological organisms in the waters.

It is possible to accurately measure transport, for example through stream tracer experiments. The method consists of instantaneously injecting a known amount of solute at some inlet point upstream of the flow and then waiting further down for the solute to come out at the outlet, at a given distance from the inlet. In particular we can measure the concentration of solute in the water over a period of time at the outlet. If we normalise the maximum concentration to one, we can expect it to have low values at the beginning, when solute has not yet reached the outlet, and then grow with time until reaching one, when all the solute is inside the basin (as qualitatively shown in figure 1.1a). This type of plot is called breakthrough curve (BTC), and – as we will see later on – it can be put in correlation with the probability of a particle to be at the outlet at a given time. We might be interested also in the discharge rate of water at the outlet. The plot of water discharge over time is called a hydrograph and gives an idea of the network responds to different inputs of water. Often a case is considered where the input is in the form of unitary rainfall volume injected instantaneously all over the network, this is referred to the instantaneous unit hydrograph (IUH). We can mention that in this kind of plot the area under the IUH curve must always be 1 (or in general the input amount) to guarantee mass conservation. Some qualitative examples of these curves can be

found in figure 1.1b.

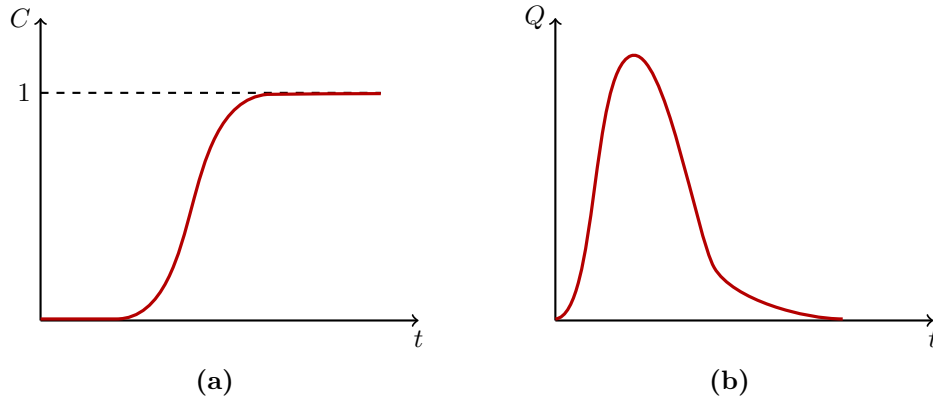


Figure 1.1: Qualitative behaviour of (a) a breakthrough curve (BTC) and (b) an instantaneous unit hydrograph (IUH) over time.

Let us now review the physics of some transport mechanisms, that are simultaneously in action during water flow (Runkel and Bencala 1995). The first one that comes to mind when thinking about a river is the downstream current. In this process, called advection, mass is transported downstream at the mean flow velocity. This movement is due the gravitational force that makes water flow from higher to lower elevations, therefore mean velocity can be easily linked to the slope of the riverbed. If for example we suppose to inject dye at a certain point in a channel, pure advection would cause the dye stain to move downstream, but it would not modify its shape. Another extremely important mechanism is dispersion. The term dispersion can indicate several different phenomena which all have the effect of spreading out the dye stain of the previous example without moving it. In terms of concentration curves, we can state that advection determines the mean of travel times while dispersion is responsible for the variance (see fig. 1.2).

All processes that produce a spread in the travel times are therefore considered dispersion mechanisms. These can be classified according to the scale at which they contribute and to the factors that cause them (Di Lazzaro et al. 2016). Hydrodynamic dispersion is a microscopic phenomenon influencing the variance of travel time at the scale of the individual channel. This mechanism is itself the combination of two transport processes, a diffusion-driven one and a shear-driven one. Molecular diffusion is due to random thermal motion of particles, which causes a flux from high to low concentration areas. Since the timescales of molecular diffusion are extremely long, its role can be significant when flow velocity in the channel is very slow, but it is normally exceeded by other phenomena. Shear-driven dispersion, instead, occurs in presence of a velocity profile in the stream; indeed in this case variations of vertical and horizontal velocities result in a significant

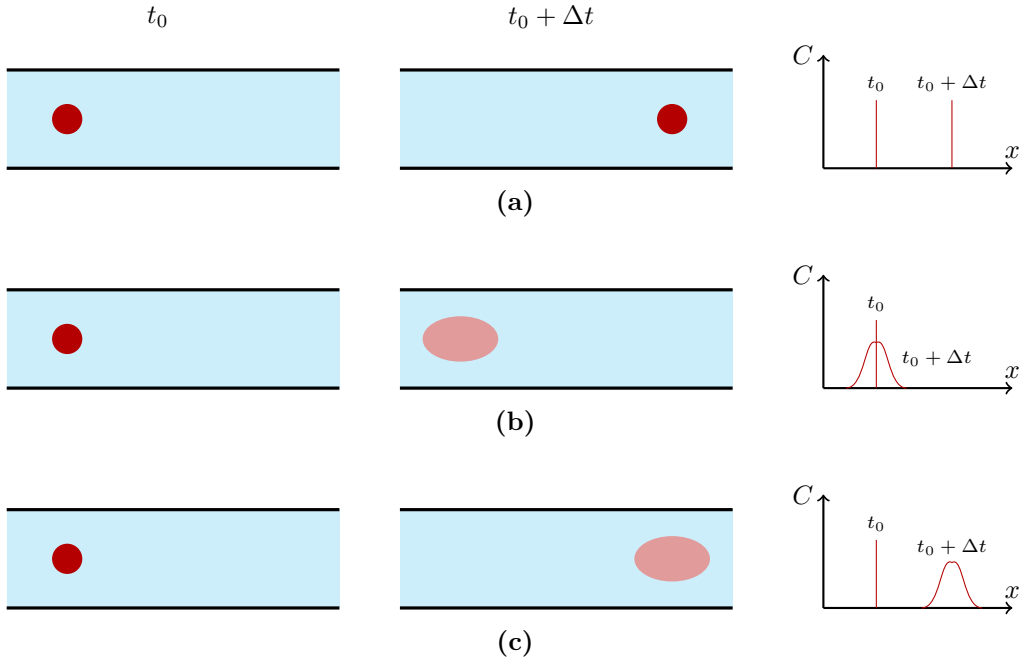


Figure 1.2: Schematic representation of the effects of (a) pure advection, (b) pure dispersion and (c) a combination of both on a dye stain introduced in a channel.

mixing of particles.

More often than not, rivers are characterised by turbulent water flow rather than laminar. This depends on slope and depth of the channels, but also on the riverbed roughness: a strong presence of sediments can trigger the transition from laminar to turbulent (Malverti et al. 2008). Large velocity fluctuations are an intrinsic property of this flow regime and give origin to macroscopic random motions that have a high spreading effect over solutes. This process is known as turbulent dispersion (Bouchez et al. 2010).

At the basin scale dispersion can be produced in different ways. An extremely important dispersion mechanism for river networks, as well as the focus of this thesis work, is geomorphological dispersion (Rinaldo, Marani, et al. 1991). This type of dispersion is related to the presence of heterogeneities in path lengths. Indeed if channels have non uniform geometric properties, solute particles have a multitude of possible paths to follow and a different choices of the path result in different travel times for the particles. Geomorphological dispersion will be described in greater detail in the next section.

If we consider instead a network where all channels have the same length and cross section but spatially varying flow conditions (velocity, for example), a dispersive contribution comes up, called kinematic dispersion. This can be divided

in two components. Channel kinematic dispersion is due to velocities being different between one channel and the other; under some conditions this contribution is comparable to the geomorphological one (Botter and Rinaldo 2003). On the other hand, hillslope-based dispersion is caused by variations in the hillslope responses of the catchment. Saco and Kumar (2002) have shown that this mechanisms can both reinforce or counteract geomorphological dispersion.

The processes we have presented so far take place within the main stream. Another class of transport mechanisms takes in consideration phenomena that become relevant when the river banks are highly permeable, which is the case for many natural streams. Lateral inflow (and outflow), for example, indicates the runoff of water contained in the soil around the channel to the main stream (or viceversa). Spatial variability in the runoff production can result in a variance contribution as well (Di Lazzaro et al. 2015; Di Lazzaro et al. 2016). This can occur for example in cases where infiltration processes or hillslope saturation present very different values in different areas of the catchment. The mechanism is known as productivity dispersion.

Transient storage is a transport mechanism related to water exchanges including two phenomena. The first, called in-channel storage, is associated to the exchange between the main flow and dead-zones (like eddies or pools); indeed water velocity is slower. and hyporheic flow, which is the exchange between water in the channel and water underneath the streambed sediments (Gooseff, LaNier, et al. 2005). Transient storage is responsible for the long tails in some breakthrough curves; indeed when solutes get ‘trapped’ in zones of slower flow, this mechanism acts so that they are released in the main channel, therefore these solutes can reach the outlet with some delay compared to the substances that did not get trapped.

1.2 Effect of the network on dispersion

We now look a little deeper into the concept of geomorphological dispersion.

Let us consider an ideal river flow where we suppose to neglect hydrodynamic dispersion and only have advection processes. We instantaneously inject some known amount of solute at the inlet, and trace it when it reaches the outlet. If our river is a stream composed of a single straight channel, water only flows straight in the downstream direction and the substance reaches the outlet all at once. The IUH curve at the outlet is still a pulse function, just like at the inlet; in particular the outcome would be as in the first example of figure 1.3.

If instead our network is more complex, composed of several branches of different lengths splitting and intersecting, then despite the absence of hydrodynamic dispersion, the outcome would be more similar to a spread out curve, like in figure

1.3. We can explain this by following substance during its travel through the river and seeing what happens. At every bifurcation mass is split (most likely in an asymmetric way) and different particles take different paths to reach the outlet. Because of the asymmetry of the network and of the varying length of the river branches, paths will have different lengths as well. Then, even if we suppose the flow velocity to be constant in the whole network, different particles will reach the outlet at different times, depending on the path they followed.

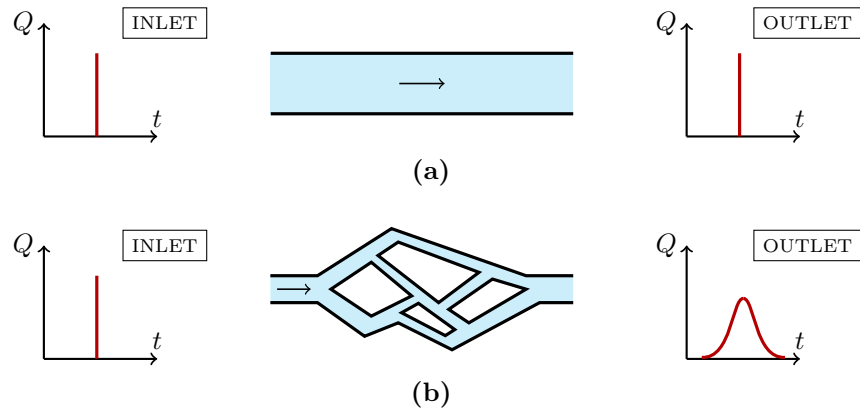


Figure 1.3: Schematic explanation for the concept of geomorphological dispersion. (a) In a straight channel where only advection is considered, an pulse injection at the inlet results in an pulse discharge rate at the outlet. (b) If once again only advection is considered, but the river network presents a more complex structure, one can observe a time spread in the measured outlet discharge rate. This must be attributed to a dispersion mechanism related exclusively to the network geometry.

Looking again at figure 1.3, we can see that the IUH variance is larger in the case of the more complex channel network; as we have said, the processes that contribute to the variance of the IUH are accounted as dispersion mechanisms. In this case the only factor that can influence the result is be the network geometry. This explains the concept of geomorphological dispersion: a term that sums up to the other dispersion contributions, but is entirely due to the geometry of the network.

Including geometric characteristics of a fluvial basin into the assessment of the IUH, gave origin to what became known as the geomorphological instantaneous unit hydrograph (GIUH) theory (Rodríguez-Iturbe and Valdés 1979). More in general GIUH theory aims to establish how a catchment reacts when subject to rainfall events and more specifically in what measure this reaction can be ascribed to the network morphology (shape, dimension...). Ideally one would be able to sum up the behaviour of the network in the hydrological response function (HRF), which combined with the rainfall input distribution returns the flow rate at the outlet. The HRF contains all the information on how the flow is affected by different factors

during the travel from inlet to outlet (Rinaldo and Rodriguez-Iturbe 1996). We can choose which transport mechanisms we want to include in the HRF, depending on the aim of the study.

The hydrological response function is actually just the specific application to hydrology of a wider concept. Indeed in general by response function one indicate a mathematical representation for the dynamic response of a system on a generic input. In particular this means that the function is able to reproduce the system behaviour in terms of output for different possible inputs. This is vastly used in electronics, especially in control and signal theory.

1.3 Braided rivers

In this section we provide a brief introduction to braided rivers, which – as we have said – constitute the object of our study.



Figure 1.4: A well studied example of braided river: River Brahmaputra in Tibet, India and Bangladesh. Photo credit: Google Earth/patternsofnatureblog.com.

Several classifications for natural riverbeds morphologies have been offered throughout the 19th century using different criteria and parameters. Rosgen (1994) proposed an extremely detailed classification and identified 8 types of patterns, divided in numerous subcategories, that can be ordered so that they are connected within a continuum.

In general (Alabyan and Chalov 1998; Kleinhans 2010) we can reduce ourselves to three main categories of river morphologies: straight, meandering and branched

(fig. 1.5). Pattern formations depend on many factors, but primarily on sediment characteristics and flow strength.

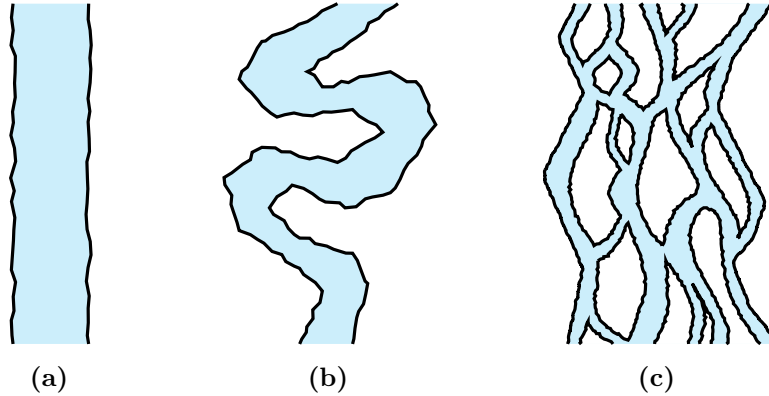


Figure 1.5: Three main categories of river morphologies: (a) a straight channel, (b) a meandering river and (c) a braided network.

In our study we have chosen to address specifically braided rivers, a class of fluvial networks that stands out for its complex and fascinating morphology. A braided river is defined as a network of multiples interconnected channels, divided by emerging sedimentary deposits. This type of river is formed in presence of very strong flow and large load of unconsolidated sediment (like sand or gravel). Furthermore braided rivers are usually formed in large unconfined valley settings and present rather high bank erosion rates (Kleinhans 2010; Connor-Streich 2019; Schuurman 2015). All these conditions allow the formation of bars in between channels; said bars are formed through depositional and erosive mechanisms and are usually free of vegetation (Ashmore 1991).

Erosion and sediment transport contribute to make braided networks extremely dynamic systems. In particular bars may shift in downstream direction, change shape, merge with one another or split, be cleared away or be created. Thus the active channels, where water is flowing, keep rearranging themselves and modifying their geometry. Some branches may be abandoned (a process known as avulsion) and possibly reactivated afterwards. Summing up, the river morphology is in constant evolution (Schuurman 2015) but its behaviour is extremely unpredictable. This complex dynamism can be very problematic in establishing appropriate management for fluvial networks, therefore numerical modeling of braided river morphodynamics has become a highly investigated topic in the last 30 years (Williams et al. 2016), ever since the seminal work of Murray and Paola (1994). Despite it being one of the most interesting features of this fluvial class, in this thesis work we will always neglect morphology evolution. Indeed the time scales of these processes are in the order of years, much larger than the ones of the dispersive phenomena of our

interest, which are in the order of minutes or hours. Therefore the two phenomena do not influence each other and we can freely suppose a fixed network for our purposes.

In addition to change of morphology it is interesting to mention that apparent changes in the network distribution can be observed by varying the water discharge. Indeed due to spatial variations of the bed elevation, higher water surface levels will cover the emerging bars until the extreme case of a single-channel stream in a high water load event; on the other hand, lowering the water level will expose more and more bars showing the multi-channel nature of the river.

Key elements composing a channel networks are bifurcations and confluences (Ashmore 1991; Schuurman 2015). In chain-like configurations such as braided rivers, they must be present with similar frequencies, which leads the average number of parallel channels per river reach to stay roughly the same (Hiatt et al. 2019). Bifurcations and confluences are the elements where distribution of both water discharge and sediment transport is determined. A rich schematic of these elements can be found in Marra et al. (2013). At bifurcations, the flux is usually partitioned in an asymmetrical way; this lack of symmetry is directly related to channel instability (Schuurman 2015). This is due to the fact that, when the discharge division becomes more and more asymmetrical, one of the two outgoing branches will probably be obstructed by sediment and abandoned by the water flow at some point, thus eliminating the bifurcation at all. Furthermore together with sediment transport bars movement and erosion phenomena also have a strong influence on the evolution of bifurcations and confluences.

The short qualitative physical description of braided rivers we have given can be useful to understand their nature, why they exist and how they are different from other types of networks. On the other hand, some quantitative notion is necessary to develop numerical models, especially considering the fact that a these networks can often be so complex that some information remains unavailable. We mention here some significant parameters when dealing with braided rivers, which try to capture important features of this type of networks.

The braiding index (BI) quantifies how intense the braiding in the river is. BI can be computed as the number of parallel channels per cross section. If only active channels are considered we talk of active BI, whereas if inactive channels are included in the count as well it is called total BI. As we have mentioned it is not always immediate to distinguish between channels and bars because river configuration changes drastically with water level, therefore usually a threshold is defined cross-sectional average bed elevation value to operate the distinction (Schuurman 2015). As pointed out in Marra et al. (2013), this parameter is useful in certain applications, but fails to capture the spatial characteristics of channels distribution.

A metric encapsulating the importance of a single channel within the whole

network is the betweenness centrality (BC). To derive this the shortest paths between any two points are computed, a channel which is part of many different paths, is more central than the others. This parameter is especially important in morphodynamics, because it tells us that changes involving a channel with high BC will have a much stronger impact on the flow than those with lower BC values.

1.4 Rivers and graph theory

In order to develop a mathematical model for GIUH theory we also need a mathematical representation of the river network. In our case a river is substituted by a directed graph. This is a data structure $G(N, E)$ consisting of a set of nodes N and a set of edges E , which link different nodes. In a directed graph (or digraph) in particular we can only move in a specific direction associated to each edge. The graph comes together with a matrix representation, the so called adjacency matrix is a square matrix of the same dimension of N , whose elements signal which nodes are connected by a link and which are not. In our study we have excluded the case of multiple links between nodes.

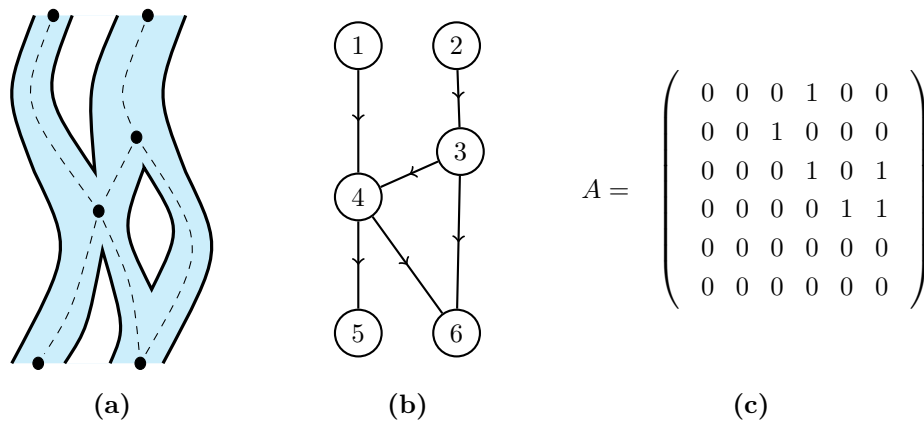


Figure 1.6: A simple example of graph extraction from a small network. (a) The actual river network: the black dots indicate the locations where we set the graph nodes. Fig. (b) shows the corresponding graph representation, with edges are directed downstream. In fig. (c) the adjacency matrix of the graph is displayed.

Going back to rivers, the representation with graphs is quite simple: each branch (or part of a branch) is associated to an edge, while nodes corresponds to bifurcations, confluences and locations in general. The direction of an edge is given by the direction of the downstream current. The cases of edges connected by multiple channels is avoided by adding extra nodes in between. A basic example can be seen in figure 1.6.

Even though the identification of rivers with directed graphs seems quite natural, so far these have been used more as conceptual frameworks rather than actual object representations (Heckmann et al. 2015; Phillips et al. 2015). Nonetheless the enormous versatility of graph theory, which is already applied to economics, neuroscience, sociology, transportation and more (Newman 2010), suggests that using network analysis to study rivers might be a good idea. Several procedures have been developed specifically for braided rivers in order to extract a graph either from imagery or from digital elevation models (Marra et al. 2013; Connor-Streich 2019; Hiatt et al. 2019). In figure 1.7 we show a simplified version of the network extraction from imagery; first a color cutoff is chosen to define the active channels, then the graph is plotted based on that.

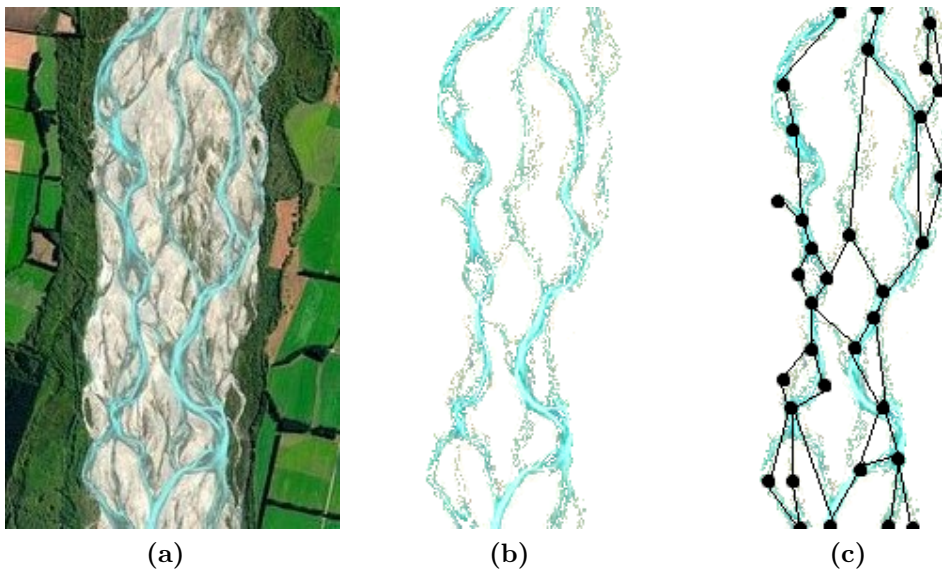


Figure 1.7: Simplified example of the extraction of a network from an image. (a) Picture of the Rakaia River in New Zealand (Photo credit: www.digitalglobeblog.com). (b) The same picture after the process of color elimination. (c) Graph representation superimposed on the river image.

Chapter 2

Mathematical model

2.1 Review of Geomorphological Dispersion

As already mentioned the bases for the concept of Geomorphological Dispersion rest primarily on the papers of Rodriguez-Iturbe and Valdés (1979) and Gupta et al. (1980).

2.1.1 Rodriguez-Iturbe's approach

In their well-known article «The Geomorphologic Structure of Hydrologic Response», Rodriguez-Iturbe and Valdés incorporated for the first time the geomorphology of the river network in a model to quantify hydrological response. This theory has become popular as the geomorphological instantaneous unit hydrograph theory (or GIUH, in short).

To give an idea of how it works, let us consider a channel network with a bucket placed at the outlet, like in figure 2.1. We suppose to inject a certain water volume at the inlet at time zero and aim to quantify the time it takes for the volume to flow through the network and fill the bucket downstream.

It is quite natural to imagine that the volume fraction flowing into the outlet at time t is equivalent to the probability that a single particle injected at time zero will arrive at the outlet at time t . Therefore the our goal can also be reached by individually following a particle in its travel from the inlet to the outlet of the river. The particle takes a certain path, with a certain probability, and its travel time will depend on the characteristics of the chosen path (the length, for example). Clearly following a single particle is not realistically achievable from a physical point of view, but this approach allows a clearer mathematical description. In this light, the initial aim of studying how fast the bucket is filled can be obtained by determining the travel time distribution of one particle at the outlet.

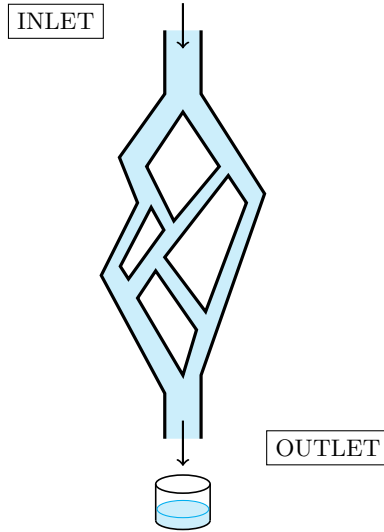


Figure 2.1: Sketch of the setting for developing Rodriguez-Iturbe and Valdés (1979)’ mathematical procedure. Water is injected instantaneously at the inlet and flows downstream through the various branches of the network until reaching the outlet, where it is collected in a bucket.

Rodriguez-Iturbe and Valdés achieved this with a probabilistic approach, more specifically in the framework of a semi-Markov process. To establish this kind of description we suppose to have a certain system that evolves from one state to another. In our case by ‘system’ we indicate the position of the particle in the network and by ‘state’ a river branch (or part of a branch). State transitions can happen at any time, and not necessarily at each time step (as would be the case in a regular Markov process). Mathematically this translates into defining both the state occupied by the system and the amount of time spent in a state as random variables.

In order to consider a semi-Markov process, we must assume a memoryless system, meaning that only the present state is used to determine the dynamics, while the sequence of all past states is irrelevant (Howard 1971). In terms of our problem, this hypothesis states that at every bifurcation the water mass splits between the two possible next branches with probabilities that do not depend on the path followed until then, but only on the present branch. In particular we will assign fixed probabilities at every bifurcation using hydraulic and geometric properties of the channels, therefore we can consider this a reasonable assumption.

The transition probability matrix \mathbf{P} must be known, which describes changes in the state of the system. If we label states with $i, j = 1, \dots, N$, each element p_{ij} is the probability that the particle enters branch j after having spent time in branch i . The notation and mathematical procedure in Rodriguez-Iturbe and

Valdés (1979) follow the ones in Howard (1971), let us briefly summarise them here, slightly simplifying the notation.

We define two different random variables representing waiting times

- T_{ij} is the conditional waiting time that the particle spends in state i before moving to j ; to this variable is associated a probability density function $h_{ij}(\tau)$.
- T_i is the unconditional waiting time, i.e. the time spent in i without knowing what will be the next state; its probability density function is given by

$$f_i(\tau) = \sum_{j=1}^N p_{ij} h_{ij}(\tau). \quad (2.1)$$

For T_i we furthermore introduce the cumulative complementary distribution

$$\bar{F}_i(t) = \int_t^\infty f_i(\tau) d\tau = \int_t^\infty \left(\sum_{j=1}^N p_{ij} h_{ij}(\tau) \right) d\tau = \mathcal{P}[T_i > t], \quad (2.2)$$

that is the probability that the particle stays in state i for more than t time.

We indicate by $\phi_{ij}(t)$ the probability for the particle to go from i to j in the interval $(0, t)$ and we aim to find a formula for it. The particle starts in i at time zero; afterwards there are two possible situations contributing to the form of ϕ_{ij} . Either the particle remains in state i the whole time until entering j at time t , or it makes a series of transitions to other states k with a final transition to j at time t . These two mechanisms can be inserted in the following fundamental equation

$$\begin{aligned} \underbrace{\phi_{ij}(t)}_{\text{prob. of going from } i \text{ to } j \text{ in time } t} &= \delta_{ij} \bar{F}_i(t) + \sum_{k=1}^N p_{ik} \int_0^t h_{ik}(\tau) \phi_{kj}(t - \tau) d\tau \\ &= \underbrace{\delta_{ij} \bar{F}_i(t)}_{\substack{\text{prob. of remaining in } i \text{ for longer than } t \\ \text{(only if } i = j)}} + \underbrace{\int_0^t \sum_{k=1}^N p_{ik} h_{ik}(\tau) \phi_{kj}(t - \tau) d\tau}_{\substack{\text{prob. of going from } i \text{ to other states } k \text{ in less than } t \\ \text{and from } k \text{ to } j \text{ in the remaining time}}}. \end{aligned} \quad (2.3)$$

Here the first term contributes only in case $j = i$ (achieved with the Kronecker delta), and represents the probability for the particle of still being in i at time t , given by the probability that waiting time in state i is larger than t . In the second term we find the product between the probability of making a transition from i to k , the probability that the waiting time in i before going to k is $\tau < t$ and the probability of going from k to j in the interval $(0, t - \tau)$.

Equation (2.3) can be easily written in matrix form

$$\Phi(t) = \bar{\mathbf{F}}(t) + \int_0^t [\mathbf{P} \square \mathbf{H}(\tau)] \Phi(t - \tau) d\tau, \quad (2.4)$$

where Φ , \mathbf{P} and \mathbf{H} are $N \times N$ matrices directly defined with their ij components, $\bar{\mathbf{F}}$ is a diagonal matrix such that $[\bar{\mathbf{F}}(t)]_{ii} = \bar{F}_i(t)$ and \square indicates the Hadamard product of corresponding elements.

We can imagine that the time spent in a branch only depends on its hydraulic and geometric properties (flow velocity, branch length...); then the next branch does not influence waiting times and we can consider T_i instead of T_{ij} . The same can be said for transition probabilities which we can define independent of time, for example using flow rates. Then it is reasonable to employ an unconditional description of the system, allowing the following simplifications

$$T_{ij} = T_i, \quad (2.5)$$

$$h_{ij}(\tau) = f_i(\tau), \quad (2.6)$$

$$\mathbf{P} \square \mathbf{H}(\tau) = \mathbf{f}(\tau) \mathbf{P}. \quad (2.7)$$

Introducing these in equation (2.4), gives us

$$\Phi(t) = \bar{\mathbf{F}}(t) + \int_0^t [\mathbf{f}(\tau) \mathbf{P}] \Phi(t - \tau) d\tau. \quad (2.8)$$

Supposing to be able to solve eq.(2.8), we can use Φ to identify the state matrix

$$\mathbf{X}(t) = \mathbf{X}(0) \Phi(t). \quad (2.9)$$

$\mathbf{X}(t)$ is a $1 \times N$ vector whose elements $X_i(t)$ represent the probability for the system to occupy state i at time t .

Finally, in order to find the probability that the particle reaches the outlet at time t we only need the component of system (2.9) relative to state $i = \text{out}$:

$$X_{\text{out}}(t) = X_1(0) \phi_{1 \text{ out}}(t) + \dots + X_{\text{out}}(0) \phi_{\text{out out}}(t). \quad (2.10)$$

For example, if we suppose to only have one inlet branch, say $i = 1$, then we are left with

$$X_{\text{out}}(t) = X_1(0) \phi_{1 \text{ out}}(t). \quad (2.11)$$

As already mentioned, this is equivalent to the water volume fraction that reaches the outlet at time t . Assuming an instantaneous injection, we would expect $X_{\text{out}}(t)$ to be close to zero for smaller t , when most of the water is in proximity of the inlet injection point, and then grow until stabilizing on 1 for larger t values, when the whole mass has reached the outlet.

We can use $X_{\text{out}}(t)$ to compute the IUH of the basin by deriving with respect to time

$$\text{IUH}(t) = \frac{dX_{\text{out}}}{dt}(t) = X_1(0) \frac{d\phi_{1 \text{ out}}}{dt}(t) + \dots + X_{\text{out}}(0) \frac{d\phi_{\text{out out}}}{dt}(t). \quad (2.12)$$

This tells us the discharge rate at the outlet.

2.1.2 Gupta's approach

Rodriguez-Iturbe and Valdés' was basically the first attempt to formalise the effects of geomorphology on travel times in a coherent theory. The following year Gupta et al. (1980) proposed a more general and conceptually simpler model. Despite the fact that we will not eventually be using this model, its clear formulation allows a deeper understanding of some concepts in the GIUH theory, especially as relates to the role of the different paths in the network. For this reason we think this review can be useful.

Gupta et al.'s model can be explained starting from a microscopical interpretation of mass balance equation. We suppose to inject in a river basin a unit volume of water, composed of a large number of non-interacting identical particles. Each particle spends a certain holding time T_B^i in the network before reaching the outlet (now superscript i stands for the particle). The volume of water in the basin at time t depends on the fraction of particles that are still in the basin at time t , i.e. the particles whose T_B^i is larger than t . We speculate that – particles being indistinguishable – all holding times are independent and identically distributed as T_B . Then, we can apply the law of large numbers finding that the needed fraction of particles is equal to the probability that T_B is larger than t . The volume in the basin at time t is then

$$V(t) = \mathcal{P}[T_B > t]. \quad (2.13)$$

Time variations of V only depend on the outflow, since the initial injection is instantaneous. Differentiating both sides of equation (2.13) with respect to t leads to

$$\frac{d}{dt}V(t) = -f_B(t), \quad (2.14)$$

where f_B denotes the probability distribution function of T_B , equal to the derivative of the cumulative distribution $F_B(t) = \mathcal{P}[T_B \leq t]$. Finally, by definition of the IUH

$$\text{IUH}(t) = f_B(t). \quad (2.15)$$

It remains now to determine $f_B(t)$, using the information on particles motion and network geometry.

There are several possible paths that each particle might choose; p_γ indicates the probability of path γ being chosen. Then

$$p_\gamma = \prod_{i \in \gamma} p_i, \quad (2.16)$$

where i are the branches composing the path. On the other hand, holding time T_B depends on the travel time of the chosen path T_γ , which is itself given by

$$T_\gamma = \sum_{i \in \gamma} T_i. \quad (2.17)$$

It follows that

$$\mathcal{P}[T_B < t] = \sum_{\gamma \in \Gamma} \mathcal{P}[T_\gamma < t] \cdot p_\gamma \quad (2.18)$$

$$= \sum_{\gamma \in \Gamma} [F_{i_{1,\gamma}} * F_{i_{2,\gamma}} * \dots](t) \cdot p_\gamma, \quad (2.19)$$

where $i_{1,\gamma}, i_{2,\gamma}, \dots$ represents the sequence of branches forming path γ and symbol $*$ indicates the convolution product between cumulative distribution functions. Then we can find the distribution function by differentiating both sides of equation (2.19), thus obtaining the IUH:

$$\text{IUH}(t) = f_B(t) = \sum_{\gamma \in \Gamma} [f_{i_{1,\gamma}} * f_{i_{2,\gamma}} * \dots](t) \cdot p_\gamma. \quad (2.20)$$

To clarify, supposing to have a Delta distribution in each branch, meaning an exact travel time rather than a spread distribution, as a result of equation (2.20) we would obtain a summation of Delta functions, one for each path γ , each peaking at T_γ and weighted by the probability to choose path γ ; a qualitative example of the resulting IUH is shown in figure 2.2.

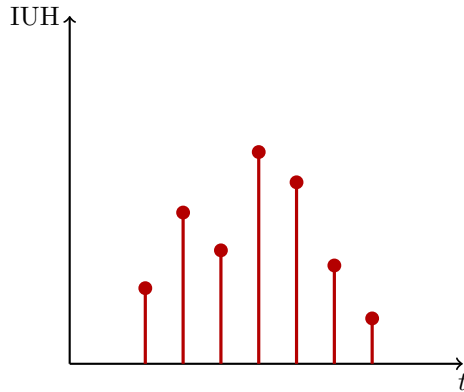


Figure 2.2: Illustrative example of the result of Gupta et al.’s model in the hypothesis of exact waiting times in each edge (delta distributions). The result is a summation of deltas, each weighted by the probability of observing the relative travel time.

A clear advantage of Gupta et al.’s model is that no restrictions must be imposed on the choice of the probability density functions; therefore they could be physically derived or assumed a priori. In their paper the authors offer two examples using uniform and exponential forms for the $f_i(t)$. On the other hand, despite apparently being simpler than Rodriguez-Iturbe and Valdés’s, this model requires the ability to compute the list Γ of all possible paths, which for a large braided network is virtually unachievable.

2.2 Further studies

The GIUH theory soon achieved great success. Many studies were published aimed at extending, perfecting or applying this theory. In this section we give an overview of these works.

A very important contribution was given by Rinaldo, Marani, et al. (1991). In their paper the authors assume Gupta et al.'s theory as a starting point and focus on developing a physical approach to derive travel time distributions. These are obtained in the Laplace domain by relating them to a $1D$ advection-dispersion equation. In the assumption of spatially invariant celerity and dispersion, an analytical form for the travel time distribution is found; in the formula parameters appear such as hydrodynamic dispersion coefficient, average path length and kinematic celerity. Furthermore Rinaldo, Marani, et al. were the ones who introduced the expression geomorphological dispersion, to indicate the other term that, together with hydrodynamic dispersion, contributes to the variance of travel times. A few years later Rinaldo and Rodriguez-Iturbe (1996) provided some extension of their previous work, reformulating the derivation of travel time distributions with a Lagrangian approach.

In Saco and Kumar (2002) the assumption of spatially invariant celerity and hydrodynamic dispersion coefficient is relaxed. Thus a third dispersion mechanism comes up, called kinematic dispersion. This is entirely due to the spatial variability of celerity in different channels and its contribution must be added to hydrodynamic and geomorphological dispersion in order to obtain the total dispersion.

Di Lazzaro et al. (2016) performed a detailed analysis to compare different dispersion mechanisms. In particular kinematic dispersion is divided in two components, one due to channel velocities, one to hillslope velocities. Their analysis focuses on the latter in particular, but to our ends it is relevant to mention that, especially in large networks, geomorphological dispersion is the prevailing mechanism.

In almost all of the works described above the study addresses converging tree-like river networks. This allows to employ some approximations for the network (Horton's laws and Strahler's orderings) that save us the need to have a complete knowledge of the river geometry; the actual network is substituted by a model. This approach was almost necessary at the origins of GIUH because then digital data for river geomorphology were not always available, especially in some areas (Rigon, Bancheri, Formetta, et al. 2016). In the case of braided rivers the same empirical laws are not valid, since the morphology is much more complex. Though some attempts have been published to obtain similar scalings and orderings also for this class of rivers (De Bartolo et al. 2022; Gleyzer et al. 2004), we have decided not to introduce such approximations in the model.

Moreover, in most cases the input is given in the form of rainfall, instantaneously

and uniformly distributed over the entire basin. These are known as rainfall-runoff models and are quite important for monitoring the quality and quantity of water into natural stream systems. Nonetheless the same models can work with a punctual injection in a specific branch, just depending on how we define initial conditions.

2.3 Residence Time Distributions

Apart from Rinaldo, Marani, et al.'s paper, which proposes a physical approach to determine travel time distributions in a single reach, the other models presented above require to specify an explicit form for said distributions. By introducing the hypothesis of exponential waiting time, for example, Rodriguez-Iturbe and Valdés have been able to simplify the equations at the point of obtaining an analytical solution. In Gupta et al.'s paper two examples were given using respectively an exponential and a uniform distribution.

We have decided to follow Rodriguez-Iturbe and Valdés' example and employ exponential distributions for the residence time in each branch. In this section we support this choice presenting some literature aimed at finding the most appropriate analytical residence time distributions (RTD) given experimental breakthrough curves.

As we have explained in the first chapter, when referring to natural streams, transient storage mechanisms give a substantial contribution to residence times dispersion (Gooseff, LaNier, et al. 2005). In particular we have mentioned in-channel storage and hyporheic exchange. The first is due to the exchange of the fast water in the main channel with dead zones (side pools or eddies), where the flow slows down and water can remain trapped. Hyporheic exchange includes the exchange between surface water and groundwater beneath streambed sediments (hyporheic zones). Generally natural streams present bed sediment and permeable banks, therefore hyporheic mass exchange occurs and realistically we should consider both contributions when modeling residence time distributions (Deng and H. S. Jung 2009). Hyporheic exchange is typically responsible for lengthening the tail of RTDs, because it traps water longer than dead zones do, releasing it later on.

Models usually derive RTDs starting from experimental breakthrough curves, obtained through stream tracer techniques. Some models require an a priori specification of the expected distribution form, which often falls on the exponential (Gooseff, Wondzell, et al. 2003), some other allow to avoid this upfront choice (Deng and H. S. Jung 2009).

It has been observed (Gooseff, Wondzell, et al. 2003) that for small streams, regardless of the reach geomorphology, the exponential RTD shows a good correspondence in shorter time periods, but it fails to capture the tail of the distribution,

meaning that solute released after a while is not well detected. In this case a power-law RTD constitutes a better choice. As we have said, a long tail should mainly be due to hyporheic exchange.

Gooseff, Wondzell, et al. (2003) were able to separate the contribution of the two mechanisms with an experiment on two different reaches of the same river. In the first reach the bed had been cleared from debris by an alluvial event; thus making it naturally subject to in-channel storage only. The second reach, of similar length, presented alluvium on the riverbed, which would cause hyporheic exchange as well. Performing a long-timescale experiment, the authors found that breakthrough curves in the first reach had short tails, to be ascribed to water coming from the in-channel dead zones; in this case RTDs were better approximated by exponentials. On the other hand in the second reach hyporheic exchange was also present, tails were much longer and power laws would give a much better fit.

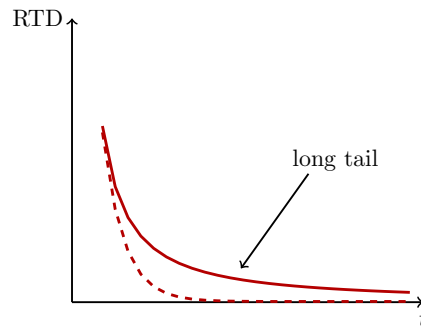


Figure 2.3: Qualitative comparison of residence time distributions (RTDs) obtained using a power-law distribution (continuous line) and an exponential distribution (dashed line). The long tail of the power-law-type curve is highlighted.

Summing up, we can neglect hyporheic transport if we choose to consider small streams with relatively smooth riverbeds; moreover we can imagine the timescale of hyporheic exchange to be quite different from the one of geomorphological mixing processes, that constitute our object of interest. In conclusion it seems reasonable for us to adopt exponential time distributions to further develop the model as in Rodriguez-Iturbe and Valdés (1979).

2.4 Model

The mathematical model we employed in this thesis work follows the one of Rodriguez-Iturbe and Valdés. This spared us the need to compute all possible paths between inlet and outlet (Gupta et al. 1980; Rinaldo, Marani, et al. 1991), which would have been particularly problematic in the case of a braided network.

Furthermore the matrix form of the equations in Rodriguez-Iturbe and Valdés (1979) is well suited to the graph representation of the river network that we intend to employ. As we have explained each edge of the graph is a river channel – or part of it – and nodes are in correspondence to bifurcations and confluences. We suppose the network to be fixed, thus ignoring changes in the morphology. From now on we will use without distinction the terms graph and river network and the terms edge and channel.

The main difference with Rodriguez-Iturbe and Valdés’ model is the interpretation that must be attributed to the states. In their paper Strahler’s ordering is applied to the network and a state is associated to the order of a stream. As for our case, since stream ordering in braided rivers is extremely complex (Gleyzer et al. 2004), each state corresponds to an edge of the graph. The semi-Markov probabilistic approach is very general, so that there are no restrictions on adopting this interpretation.

We assume the waiting times to be exponentially distributed in each channel. This hypothesis is justified by the explanation in the previous section and is essential for reaching an analytic solution (as done in Rodriguez-Iturbe and Valdés 1979; Howard 1971). If by N we indicate the total number of edges in the graph, labeled $i = 1, \dots, N$, then introducing exponential forms means defining the unconditional waiting time distributions and the cumulative complementary distributions respectively as

$$f_i(t) = \lambda_i e^{-\lambda_i t}, \quad \bar{F}_i(t) = \int_t^\infty f_i(\tau) d\tau = e^{-\lambda_i t}. \quad (2.21)$$

Parameter λ_i represents the inverse of the mean holding time in channel i . The qualitative behaviour of these functions is shown in figure 2.4. We now need to insert these exponentials into equation (2.8) to further develop the calculations.

Let us proceed as in Howard (1971) and transfer our computation in the Laplace domain through the transform $\mathcal{L}[g](s) = \hat{g}(s) = \int_0^\infty g(t)e^{-st} dt$, defined in variable s . Then the functions in equation (2.21) transform into

$$\hat{f}_i(s) = \frac{\lambda_i}{s + \lambda_i}, \quad \hat{\bar{F}}_i(s) = \frac{1}{s + \lambda_i}. \quad (2.22)$$

We transfer equation (2.8) in the s -domain exploiting some properties of the Laplace

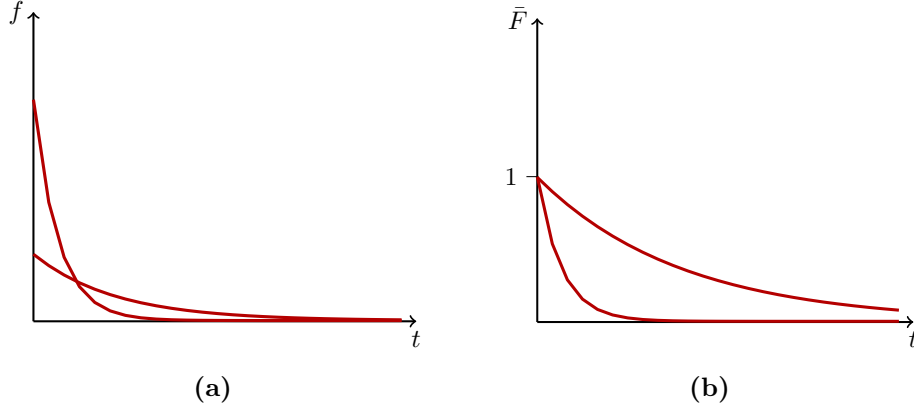


Figure 2.4: Qualitative behaviour of the exponential forms of (a) the unconditional waiting time distribution $f_i(t)$ and (b) the cumulative complementary distribution $\bar{F}_i(t)$, as described by eq. (2.21).

transform

$$\Phi(t) = \bar{F}(t) + \int_0^t [\mathbf{f}(\tau)\mathbf{P}] \Phi(t - \tau) d\tau, \quad (2.23)$$

$$\implies \hat{\Phi}(s) = \hat{F}(s) + \hat{\mathbf{f}}(s)\mathbf{P} \hat{\Phi}(s) \quad (2.24)$$

$$= [\hat{\mathbf{F}}^{-1}(s) - \hat{\mathbf{f}}(s)\mathbf{P}]^{-1} \quad (2.25)$$

$$= \left[\begin{bmatrix} \ddots & & 0 \\ & s + \lambda_i & \\ 0 & & \ddots \end{bmatrix} - \begin{bmatrix} \ddots & & 0 \\ & \frac{\lambda_i(s + \lambda_i)}{s + \lambda_i} & \\ 0 & & \ddots \end{bmatrix} \mathbf{P} \right]^{-1} \quad (2.26)$$

$$= [s\mathbf{I} + \mathbf{\Lambda} - \mathbf{\Lambda}\mathbf{P}]^{-1} \quad (2.27)$$

$$= [s\mathbf{I} - \mathbf{\Lambda}(\mathbf{P} - \mathbf{I})]^{-1} \quad (2.28)$$

$$= [s\mathbf{I} - \mathbf{A}]^{-1} \quad (2.29)$$

where $\mathbf{\Lambda} = \begin{bmatrix} \lambda_1 & \dots & 0 \\ \vdots & \ddots & \vdots \\ 0 & \dots & \lambda_N \end{bmatrix}$ is the diagonal matrix containing the inverses of mean holding times and $\mathbf{A} = \mathbf{\Lambda}(\mathbf{P} - \mathbf{I})$ is called the transition matrix.

The great advantage of the expression in equation (2.29) lies in the fact that it allows analytical anti-transform in time domain. Therefore we end up with the following closed form for matrix $\Phi(t)$, i.e. the probability of going from one edge

to another in time t :

$$\Phi(t) = e^{\mathbf{A}t} = \mathbf{I} + \mathbf{A}t + \frac{\mathbf{A}^2 t^2}{2!} + \dots \quad (2.30)$$

which we can finally insert in equation (2.9) to find the solution for $\mathbf{X}(t) = \mathbf{X}(0)\Phi(t)$, probability for the particle of being in a certain state at time t . In particular, when limiting ourselves to the columns relative to outlet branches, we can write

$$X_{\text{out}}(t) = X_1(0) [e^{\mathbf{A}t}]_{1 \text{ out}} + \dots + X_{\text{out}}(0) [e^{\mathbf{A}t}]_{\text{out out}}. \quad (2.31)$$

For the IUH we can differentiate the equation above and exploit the fact that $\frac{d}{dt}e^{\mathbf{A}t} = \mathbf{A}e^{\mathbf{A}t}$, thus obtaining

$$\text{IUH}(t) = X_1(0) [\mathbf{A}e^{\mathbf{A}t}]_{1 \text{ out}} + \dots + X_{\text{out}}(0) [\mathbf{A}e^{\mathbf{A}t}]_{\text{out out}}. \quad (2.32)$$

Matrix \mathbf{A} contains the information on the network: the mean waiting time for each branch (\mathbf{A}) and the existing links between them (\mathbf{P}); while the components of vector $\mathbf{X}(0)$ tell us how the initial instantaneous input is distributed in space.

In particular if we consider the case of a network with a single inlet and a single outlet channel, we are left with

$$\text{IUH}(t) = X_{\text{in}}(0) [\mathbf{A}e^{\mathbf{A}t}]_{\text{in out}}. \quad (2.33)$$

Once the IUH is computed, we find ourselves in possess the network response function. With this we can easily know the values that reach the outlet as a consequence of any input function, by performing a time convolution between the IUH and the initial distribution $i_0(t)$; this is called the ‘response’ of the network. At the outlet we will then have the following discharge

$$Q(t) = \int_0^t \text{IUH}(t - \tau) i_0(\tau) d\tau. \quad (2.34)$$

Let us recall that differently from most works, where i_0 is given as spatially uniform rainfall, in our case the input distribution refers to one inlet branch exclusively.

To cover the case of multiple entries and multiple exits, we can generalise the approach. We start by computing multiple IUHs, one for each inlet-outlet combination $\text{IUH}_{\text{in}_i \text{ out}_j}(t)$ with the model presented until now. Afterwards we convolve every $\text{IUH}_{\text{in}_i \text{ out}_j}(t)$ with the initial distribution at the relative inlet in_i , thus obtaining a $Q_{\text{in}_i \text{ out}_j}(t)$ representing the contribution at outlet out_j due to the injection in inlet in_i . Finally we can sum over the inlets to find a $Q_{\text{out}_j}(t)$, which gives us the total discharge at outlet out_j as a consequence of all different inputs. This allows us to have, together with the time spread of each discharge, a knowledge of the spatial distribution of the injected volume among all possible outlets.

Chapter 3

Results

In order to validate the theoretical model described so far, we have performed some numerical simulations aimed at pointing out the most interesting features of the GIUH theory. The mathematical model of chapter 2 was implemented in MATLAB and applied to small networks with realistic geometries. In this chapter we summarise and remark on the results thus obtained.

3.1 Toy networks

We start by quickly showing the results of an ad-hoc built experiment, aimed at illustrating the basic features of geomorphological dispersion. The experiment can be described as follows.

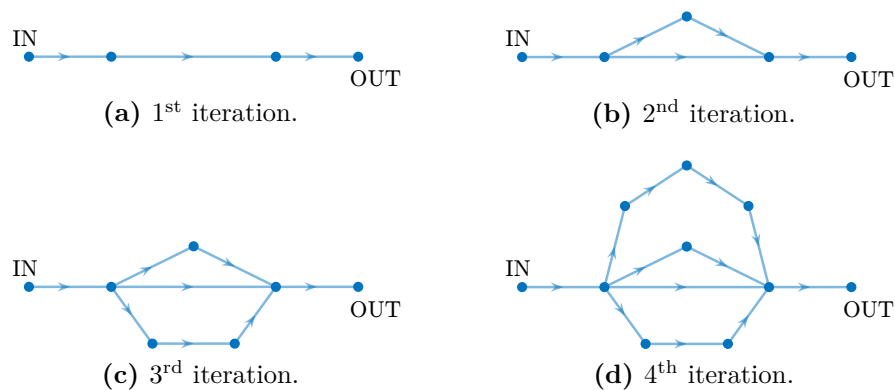


Figure 3.1: Toy graphs are formed by keeping inlet and outlet fixed and adding a new path of different length between them at every iteration. So that the first graph (a) only has 1 path of length 1, the second (b) has an extra path of length 2, the third (c) an extra path of length 3, and so on.

We generate a graph consisting of three edges, respectively an inlet, an outlet and a link between them. Notice that this network represents a straight channel. We compute the IUH of this network, which gives us the outlet discharge rate in response to the introduction of a delta distribution at the inlet. Then, keeping the existing network fixed, we add two new edges forming a second path between the inlet and the outlet and compute again the IUH of the new network. We continue this process so that at the n^{th} iteration we add a path formed of n edges, finding ourselves with a total of n different paths with lengths going from 1 to n . At each iteration we also compute the IUH. Figure 3.1 illustrates how the graphs are created.

The aim of this experiment is observing the changes in the IUH as the number of available paths and path lengths increases. Considering what we explained in section 2.1, we would expect the IUH to spread out over time when the network grows. Quantitatively this must be reflected by the IUH variance values, which should increase along with the number of paths.

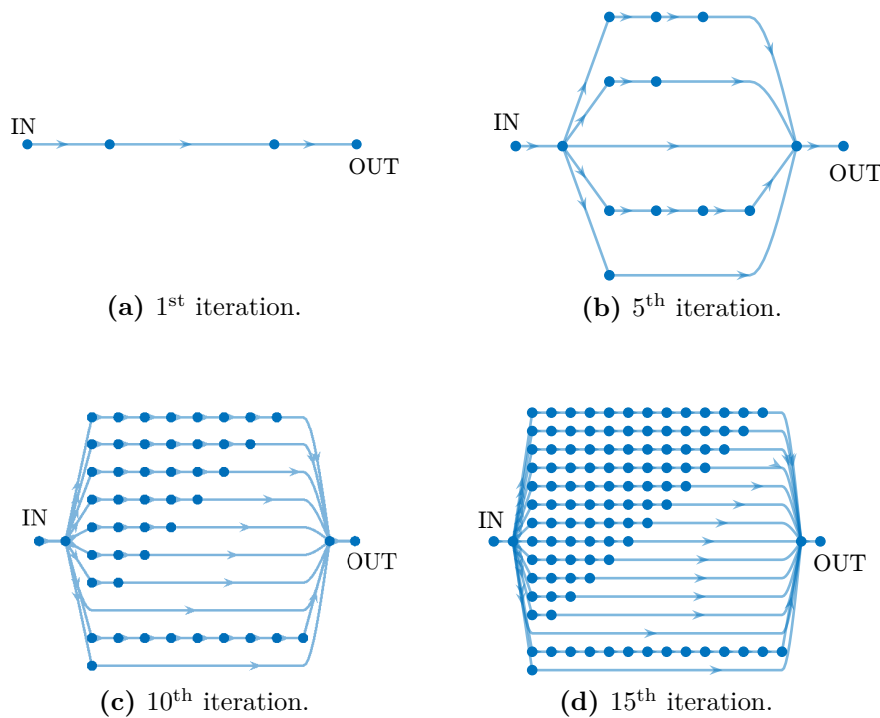


Figure 3.2: Toy graphs for the simulations whose results are shown in fig. 3.3.

In order to verify this we perform 15 iterations of the process and attribute travel times equal to 1 to all edges. In figure 3.3 we report the results referring to four iterations only, for the sake of clarity. The black dashed lines represents

an input delta function, to remind us that the IUH coincides with the network response to the introduction of this kind of distribution. The blue lines are the IUHs curves, they all present different line pattern since they each refer to a different iteration, as explained in the legend. Looking at the IUHs we observe that, as the iteration number increases, the peaks lower and the curves spread out over the horizontal axis. This is confirmed by the values of the parameters indicated within the legend. Indeed at higher iterations, as the number of possible path lengths grows, both the mean travel time and the variance value show a clear increase. This is exactly the concept of geomorphological dispersion that we gave: a larger number of possible paths and path lengths determines a spread in the travel times at the outlet. Therefore we must attribute this dispersion contribution to the network geometry.

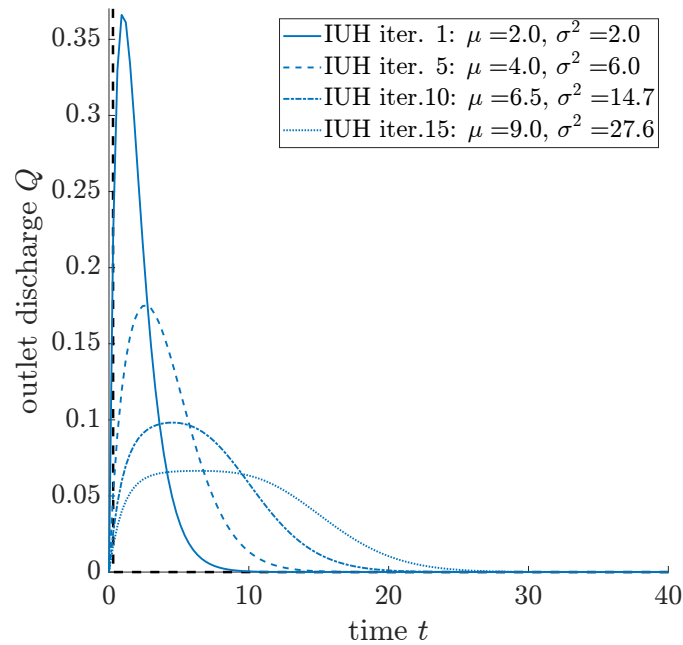


Figure 3.3: Resulting IUHs from four iterations 1, 5, 10 and 15 of the toy experiment; the graphs are shown in fig. 3.2. The black dashed line represents the input delta distribution and the blue lines are the IUHs of the different networks.

3.2 The Borbera network

The simulations are performed on networks relative to a reach of the Borbera Stream, in Southern Piedmont. A graph representation of this river reach (fig. 3.7), extracted in a previous work using DEM data, has been made available by the Department of Environment, Land and Infrastructure Engineering (DIATI) at Politecnico di Torino.

3.2.1 Site description

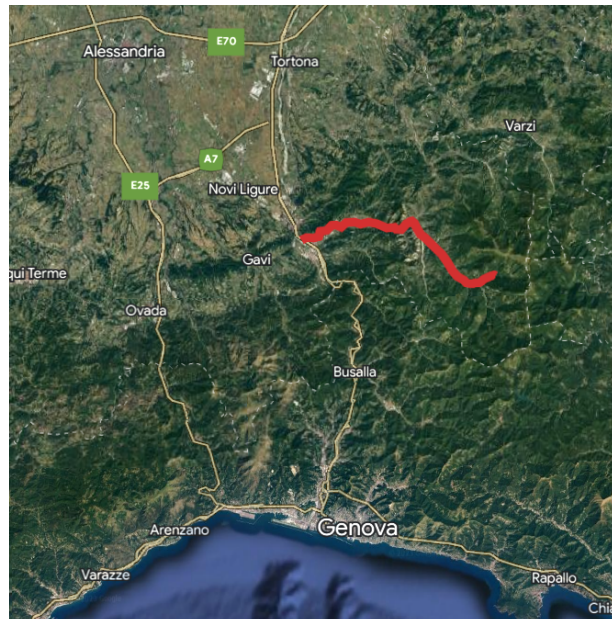


Figure 3.4: Geographic location of the Borbera Stream. Image produced with Google Earth software.

The Borbera Stream is a small river located in the south of the Piedmont region, in the province of Alessandria. The Borbera originates on the Ligurian Apennine, between Mount Chiappo and Antola and follows a course of approximately 38 km, until the confluence into the Scrivia River. The hydrological regime of the Borbera is the typical regime of a mountain river, with very wide seasonal variations with heavy flow rates in spring and autumn.

3.2.2 Graph description

As we have explained in chapter 1, the active river channels change according to the values of the average flow rate, and this result in different graph geometries.



Figure 3.5: Zoom of a braided reach in the Borbera Stream. Both active and inactive channels are visible. Image produced with Google Earth software.

Several networks had been made available, for different values of flow rate, velocity and water level threshold. We chose to use only the network obtained with flow rate equal to $45 \text{ m}^3 \text{ s}^{-1}$, since in this case we find ourselves with only one connected component.

The full network is shown in figure 3.6. It is composed of $N_n = 3212$ nodes and $N_e = 3800$ edges. The majority of network elements consist in bifurcations (590) and confluences (589) where two edges are involved, nevertheless few splits with three or four channels can be identified (30 ingoing and 35 outgoing). Water flows from left to right. The graph comes with a directed adjacency matrix of

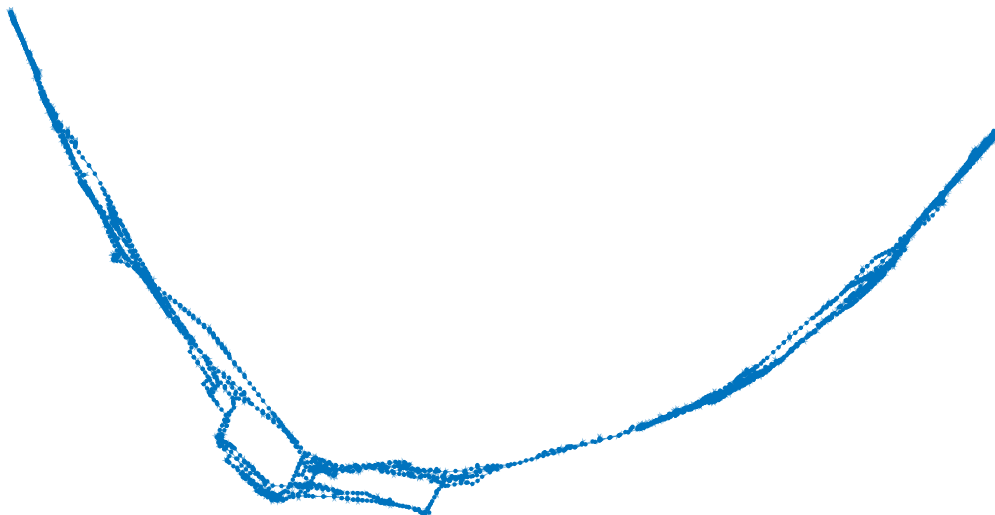


Figure 3.6: Entire available graph representation of the Borbera network. Water flows from left to right. This network consists of $N_n = 3212$ nodes and $N_e = 3800$ edges.

dimensions $N_n \times N_n$, which turns out to be sparse given that only $N_e = 3800$ matrix

elements are nonzero. From this description we can easily move to an edge-driven one by building a matrix R of dimensions $N_e \times N_e$, whose elements R_{ij} are equal to 1 if edge i outlet node coincides with the inlet node of edge j . Matrix R is used to set the structure of P_{ij} , the probability matrix of the model. It is worth mentioning that, due to the network complexity, no ordering of the edges or the nodes is possible in the graph. In addition to this both the adjacency matrix and the probability matrix are highly sparse matrices, due to the relatively low number of links compared to the total number of edges.

Since this network is very large, we do not use it as it is, but rather extract from it smaller sub-networks to test. Thus the test-networks will have realistic geometries. On the other hand the values we assign to waiting times are not physically derived, but rather we impose values of our choice. This does not affect the dynamics of the system; in particular we can suppose that the travel times have been normalised by the factor of a typical network timescale.

3.3 Numerical simulations on a single-inlet single-outlet network

3.3.1 Network description

For the first set of simulations we extrapolate a small network from the upstream part of the network. In order to have a unique inlet and outlet, we add to the graph two dummy edges (those indicated with ‘IN’ and ‘OUT’). Consequently dummy links are inserted to connect each of them to the main network, respectively four for the inlet and six for the outlet. The resulting graph is shown in figure 3.7. It is composed of $N_n = 56$ nodes and $N_e = 68$ edges. We identify 8 bifurcations, 8 confluences and one trifurcation, in addition to the splits of four and six dummy branches. In this graph there are a total of 30 paths from inlet to outlet, the shortest consists of 6 edges, the longest of 24. These properties are summarised in table 3.1.

Property	Value
N_n	56
N_e	68
Bifurcations	10
Confluences	9
Paths	30

Table 3.1: Summary of some properties relative to the graph in figure 3.7.

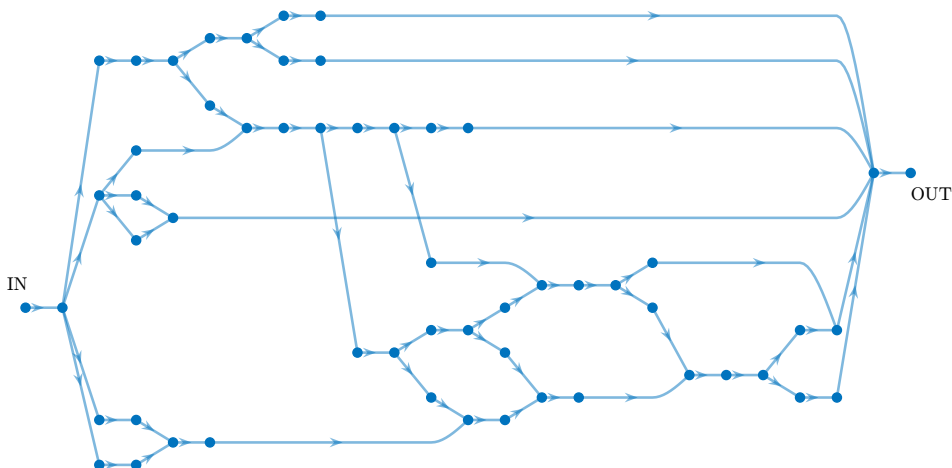


Figure 3.7: Graph with a single inlet and single outlet. The graph has been extracted from the network in figure 3.6, afterwards 2 dummy edges were added to have a unique inlet and outlet, 4 dummy links to the inlet and 6 dummy links to the outlet. Some properties of the graph are summarised in table 3.1.

3.3.2 Equal waiting times and symmetric bifurcations

For the first test, we set the average waiting time equal to 1 in each edge and suppose that mass is split equally at every bifurcation. This means that if two edges depart from a node, we attribute to each probability 0.5, if there are three edges, probabilities are distributed as 0.33 - 0.33 - 0.33, and so on. We use a time discretisation step of $dt = 0.3$ for all following simulations.

We start by computing the network response function, that is the IUH, using the model developed in chapter 2. Once the IUH is obtained, we just need to perform a numerical convolution in order to find the response of the network to any input distribution.

Figure 3.8 shows some examples of network response to different inputs. In green we represent a square function of width 9 and its response, while in orange we have a gamma distribution of the form

$$\gamma(t) = \frac{\beta^\alpha t^{(\alpha-1)} e^{-\beta t}}{\Gamma(\alpha)}, \quad \alpha = 6, \quad \beta = 0.15.$$

All input functions (fig. 3.8a) are normalised so that the area underneath equals 1; this is equivalent to injecting a volume 1 of water into the inlet. The area remains 1 in the response curves of figure 3.8b as well, ensuring mass conservation. Unsurprisingly, going through the network has a time spreading effect on all the input curves, as we can gather from the variance values σ^2 .

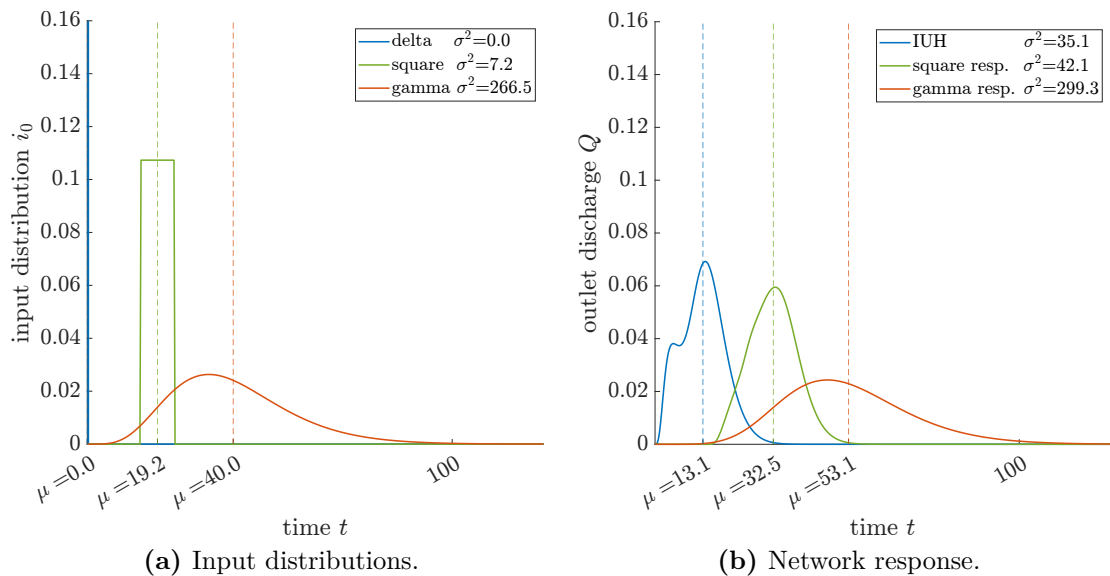


Figure 3.8: Results of the first simulation performed on the network of fig. 3.7. (a) On the left three different initial distributions to be injected in the inlet are represented. (b) The right figure shows the network response to each input distribution (with corresponding colour), obtained by convolution. The blue curve representing the discharge due to a delta coincides with the IUH of the network. Mean values of the curves are indicated by the dashed lines, while variance values are indicated within the legends.

The blue curve in figure 3.8b represents our IUH, that is the network response to the introduction of a delta distribution. We can observe that the mean of the IUH is located at $t = 13.1$ and that the curve completes its descent around $t = 27$, consistently with the fact that the longest path is composed of 24 edges (we recall that each edge has a mean waiting time of 1).

3.3.3 Enhanced network

We can exploit the already computed IUH to reproduce with a trick the case of a larger network. Suppose to double the graph of figure 3.7 so that the outlet serves as the inlet to another network, identical to the previous one. Figure 3.9 shows the network doubled in this way. Now this new graph has roughly twice as many edges as the previous one, therefore computing its IUH from scratch – which implies computing an exponential matrix twice the size – requires a much higher computation time.

Rather than doing this expensive operation, we can just focus on the smaller graph and suppose to re-inject the outlet discharge in its inlet. This is achieved by

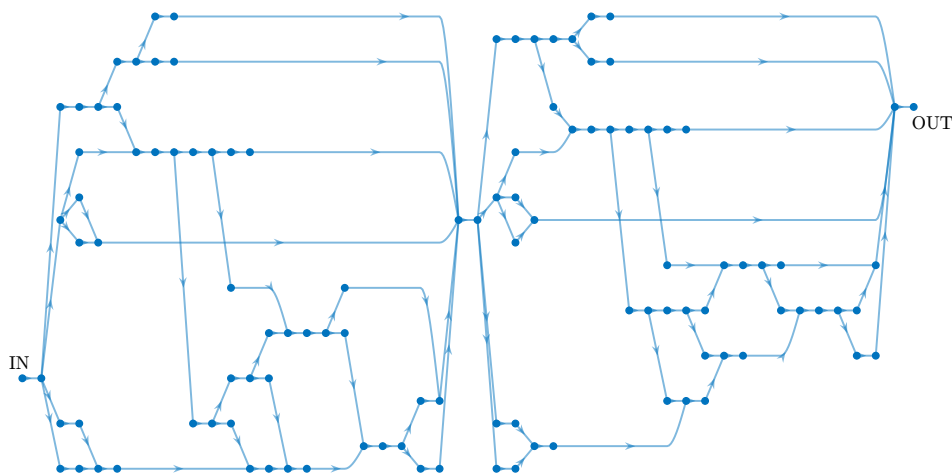


Figure 3.9: Graph obtained by ‘doubling’ the network in fig. 3.7, i.e. overlapping the outlet of a first copy of the graph with the inlet of a second copy.

performing a convolution of the known IUH with itself. Rephrasing, finding the response of the network in figure 3.9 to the introduction of a delta, is equivalent to computing the convolution between the IUH of the graph in fig. 3.7 and itself. Figure 3.10 shows the IUHs of the doubled and tripled version of the initial graph computed with this convolution trick rather than from scratch. We can now use these curves as response functions for the larger networks and convolve them with any input distribution. Unsurprisingly we observe that the IUH becomes more and more spread out by enlarging the network and that its mean value shifts to the right approximately 13.4 by 13.4.

The importance of this result lies in the fact that if we adequately choose a small river section, so that it encapsulates the average properties of the entire network (number of parallel channels, number of bifurcations...), and compute its IUH, then the function obtained with the convolution trick will be a good approximation of the actual response function of entire network. But this procedure saves us the expensive computation of a large exponential matrix.

3.3.4 Multiple waiting times

As a second experiment we allow waiting times to be different in each edge. We assign random values extracted from a uniform distribution in the range 0.2 - 1.9 with an average equal to 1. The new waiting time values are indicated for each edge in figure 3.11.

The resulting response curves are presented in figure 3.13a. We notice that the variance are slightly higher than those of figure 3.8b, while there is very little difference in terms of mean value.

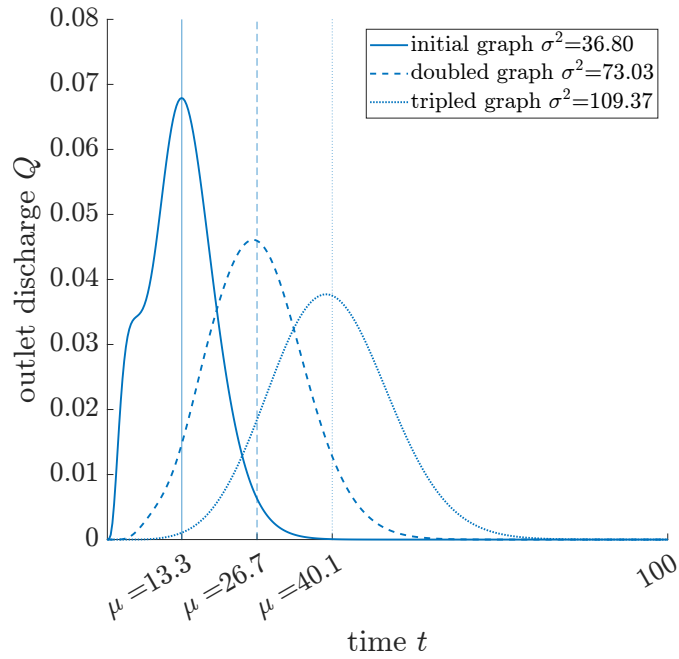


Figure 3.10: IUHs of the graph in fig. 3.7, its doubled version and its tripled version, respectively associated to the continuous, dashed and dotted blue lines. These response functions are not directly computed from large networks, but are obtained as convolutions with the of the small graph IUH with itself.

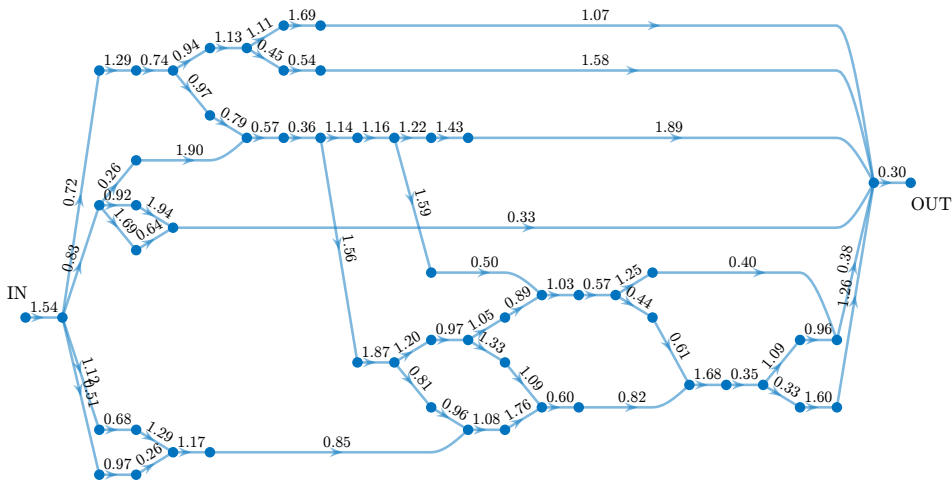


Figure 3.11: Network with the same geometry of the one in fig. 3.7, but different mean waiting times in each edge. These values are selected randomly in the range 0.2 - 1.9 so that the average is 1 and are shown on the edges in the graph.

3.3.5 Non-symmetric bifurcations

Another variation we can introduce regards the mass distribution at bifurcations. For simplicity we set again all waiting times equal to 1 and vary the probability values at bifurcations: instead of symmetric volume division like 0.5 - 0.5, we assign random values so that they add up to 1. The new non-bifurcations are shown in figure 3.12.

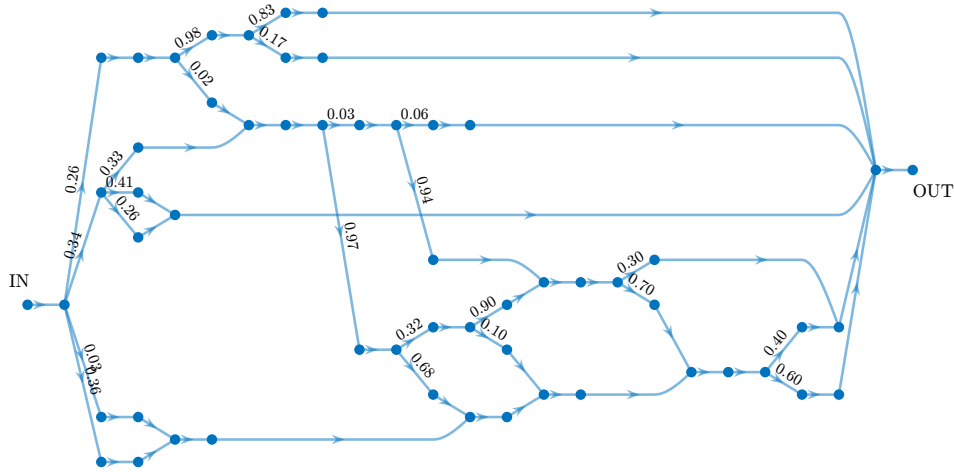


Figure 3.12: Network with the same geometry of the one in fig. 3.7, but with non-symmetrical bifurcations. The non-trivial probability values at bifurcations, randomly assigned, are indicated on the edges.

We illustrate the response curves in figure 3.13b. In this case mean values and variances are basically the same of figure 3.8b. As an effect we can observe that if that in the first test we had a smaller peak around 5, this has now become even higher than the peak at 13, due to the fact that the paths of length 5 have become more likely. Despite it not being visible in this case, a typical effect of non symmetric bifurcations is actually of reducing the response curve variance. This can be explained by understanding that if some paths have a much higher probability than others, it is almost like the number of paths – and thus their diversity – has been reduced.

3.3.6 IUH dependency on time and bifurcation values.

An interesting observation we can make with the results obtained so far concerns the relative influence on the IUH of waiting time or bifurcation values with respect to the network structure. The question we ask here is: are these parameter values really important or is the IUH mostly determined by the network geometry?

To answer this, we perform a series of numerical simulations where we randomly change the waiting times and bifurcation probabilities (first one at a time, then

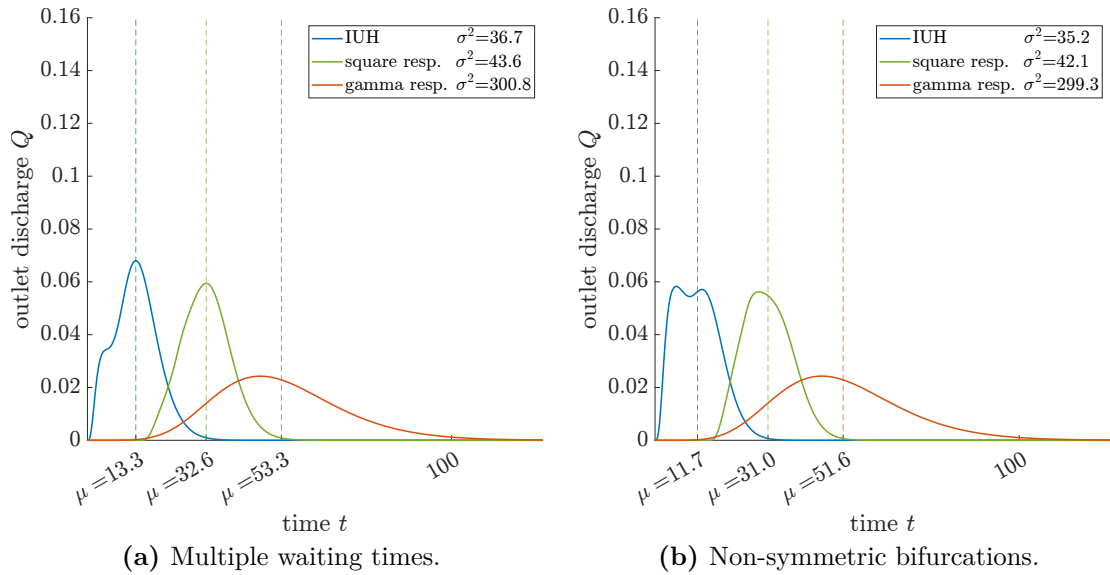


Figure 3.13: Resulting IUHs from the simulations on (a) the graph with multiple waiting times (fig. 3.11) and (b) the graph with non-symmetric bifurcations (fig. 3.12). The input distributions considered are the same of fig. 3.8a.

together) but we maintain the network fixed. For every simulation we obtain a certain IUH and, by averaging over all these curves, we find a mean IUH, which we then compare with a benchmark curve.

More specifically in our test we performed 50 simulations where we randomly varied waiting times, 50 simulations for the bifurcation values, and 50 changing both parameters at the same time. The results of these experiments are shown in figure 3.14. The benchmark case, as already mentioned, consists of a graph with waiting times equal to 1 and probability values symmetrically distributed at every bifurcation; its IUH is represented by the blue curves. The blue curve instead represents the curve obtained as the mean of all IUHs. For clarity reasons we do not plot the results of all 50 simulations; we only display the range that they cover – the yellow bars – and the value of one standard deviation, given by the dashed lines.

As we can see it seems that the the benchmark IUH and the mean curve are extremely close. To quantify this we compute the norm of the difference between them, obtaining in all cases a value of the order 10^{-2} . These norm values do not seem to depend on the number of test iterations we consider, that is the sample size, though when we increase the number of tests the spread of the sample data also increases. Table 3.2 reports some quantitative parameters relative to the benchmark IUH and the mean curves in each case. Together with the mean value and the variance, which we have already discussed, we display values for skewness

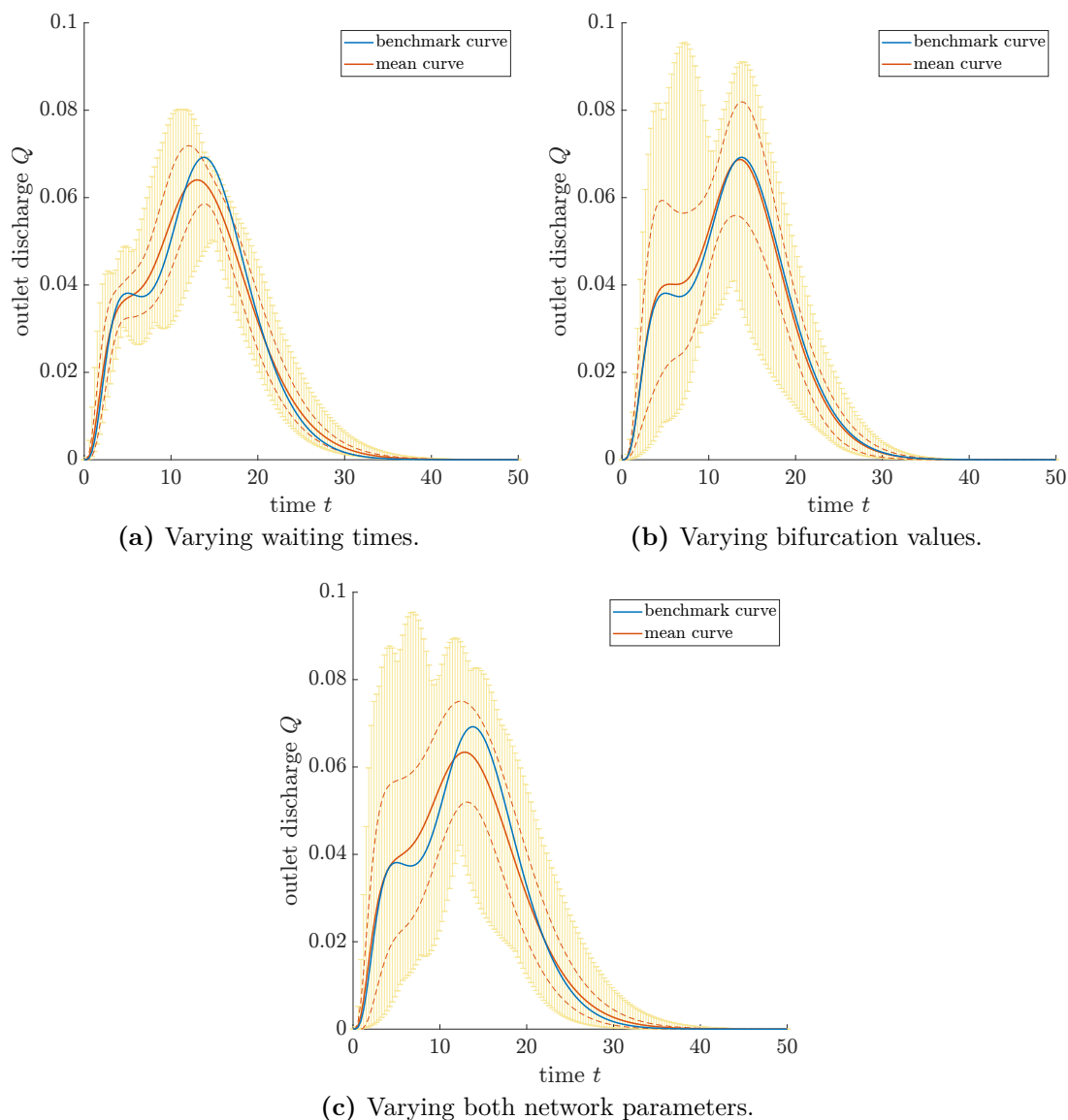


Figure 3.14: Results from a series simulations on the graph in fig. 3.7. In (a) we attribute random waiting times to all edges; (b) shows the case where random probability values are given at bifurcations; in (c) both network parameters are varied simultaneously at every iteration. For each case we perform 50 iterations. The blue curve represents the IUH of the benchmark graph (waiting times 1 and symmetric bifurcations), the orange curve is obtained as the mean of all 50 IUHs, while the yellow bars are the upper and lower envelopes and the dashed lines show one standard deviation of the IUHs distribution.

and kurtosis of the curves. The Skewness gives a measure of the curve symmetry, while Kurtosis relates to the presence of long or short tails in the data distribution.

Curve	Mean μ	Variance σ^2	Skewness	Kurtosis
Benchmark IUH	13.15	35.15	1.39	3.50
Mean curve (a)	13.16	39.42	1.30	3.17
Mean curve (b)	12.90	34.52	1.38	3.41
Mean curve (c)	13.00	39.50	1.29	3.10

Table 3.2: Some quantitative parameters for the benchmark IUH and the mean curves of each test; letters (a), (b), (c) refer to the subfigures of fig. 3.14.

3.4 Numerical simulations on a multiple-inlet multiple-outlet network

In this section we perform simulations on a network with multiple inlets and multiple outlets. The procedure to compute the discharge at the exits in this case requires a few more steps, reproducing the mathematics explained at the end of section 2.4. First we compute all the IUHs from each inlet to each outlet, in the same way as in the previous tests. Afterwards the discharge at each outlet is determined by convolution of the IUH with an input distribution function (which can be different in each inlet). Finally we combine the discharges by summing all contributions to the same outlet, and we obtain a discharge distribution for each exit. In this set of simulations we especially monitor the volume fraction reaching each outlet, in order to have an idea of the discharge spatial distribution along with the time distribution, that is how much water ends up at which outlet.

3.4.1 Network description

Like in the earlier, the graph we work on is also extracted from the initial part of the complete network. It counts 98 nodes and 110 edges, of whom 2 inlets and 3 outlets, which we indicate with numbers as shown in fig. 3.15. Table 3.3 sums up these values and specifies some more information regarding the number of paths from each inlet to each outlet. We rapidly observe that there is a big gap in the paths distribution among the exits, with a total of 16 paths leading to outlet 1 versus 6 and 6 paths to outlet 2 and 3 respectively. Of course these values must be weighted with the path probabilities too, but, if we suppose all paths equally likely, we can already foresee a tendency for injected water to reach outlet 1 in larger quantities than the others.

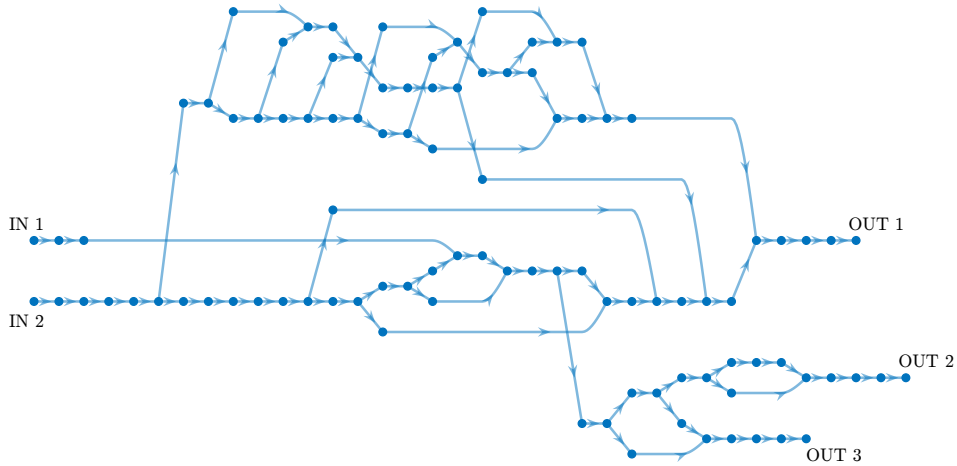


Figure 3.15: Graph with a 2 inlets and 3 outlets, extracted from the initial part of the network in figure 3.6. Here we suppose that all edges have mean waiting time 1 and at each bifurcation probabilities are distributed symmetrically among the outgoing edges. Some properties of the graph are summarised in table 3.3.

Property	Value	Inlet	→	Outlet	Paths
N_n	98	IN 1	→	OUT 1	1
N_e	110	IN 1	→	OUT 2	2
Inlets	2	IN 1	→	OUT 3	2
Outlets	3	IN 2	→	OUT 1	15
Bifurcations	14	IN 2	→	OUT 2	4
Confluences	15	IN 2	→	OUT 3	4

Table 3.3: Summary of some properties relative to the graph in figure 3.15.

3.4.2 Equal waiting times and symmetric bifurcations

Just like we did earlier we start with the case of symmetric bifurcations and equal mean waiting times in all edges.

First we suppose to inject in each inlet an amount 1 in the form a delta distribution, and we observe how this is reflected at the outlets. Figure 3.17 represents this case.

As indicated in table 3.3 the path from inlet 1 to outlet 1 is unique. Along this path there is only one bifurcation which allows a deviation to the other outlets, then 50% of the input mass must reach outlet 1 while the other half is divided among 2 and 3. This is exactly reproduced by the area values in fig. 3.17a, wich shows that the volume fraction reaching outlet 1 is equal to 0.5. Here we observe the case where a single path has a much higher probability of being covered than the other four, so it carries by itself the majority of water volume. The fact that

the path is unique also explains why the IUH is so narrow (compared for example to the blue curve of fig. 3.17b where the paths are 15); all visible time spreading in this case is due to the use of exponential laws rather than geomorphological dispersion.

For inlet 2, instead, we see from table 3.3 that there are 15 paths leading to outlet 1 and half as many leading to the other outlets. Furthermore the first three bifurcations we encounter all lead to outlet 1 directly, which attributes high probabilities to many of the 15 paths. This explains why almost all the water volume (94%) ends up at the first outlet (see fig.3.17b).

Finally the curves in figure 3.17c are obtained by summing the contributions to each outlet coming from both the inlets. In light of the considerations we made for figures 3.17a and 3.17b, it is not surprising that outlet 1 receives most of the volume.

Figure 3.18 shows the results of a test performed on the same network with symmetric bifurcations, where instead of a deltas we introduce gamma distributions. We use different parameters for the two inlets, in particular:

$$\gamma(t) = \frac{\beta^\alpha t^{(\alpha-1)} e^{-\beta t}}{\Gamma(\alpha)}, \quad \begin{array}{ll} \text{IN 1: } & \alpha = 15, \quad \beta = 0.3 \\ \text{IN 2: } & \alpha = 11, \quad \beta = 0.4 \end{array}$$

Afterwards the values are normalised so that the area under each curve – i.e. the injected volume – is equal to 1. The gamma input distributions are represented by the dashed lines in fig. 3.18a and 3.18b, for each outlet respectively. As we can see the area values reported within the legend virtually coincide with those of the previous case, this is because the volume fraction distribution only depends on bifurcations probabilities and not on the input form. We mention that the two injected distributions have quite different mean values: the first one peaks around $t = 27$ (fig. 3.18a), while the second one around $t = 50$ (3.18b). This difference in the injection times is reflected by the multiple peaks we can observe in the blue curve of figure 3.18c, where both gammas are considered simultaneously.

3.4.3 Non-symmetric bifurcations

For the second set of simulations we refer to the graph in figure 3.16. Now non-symmetric probabilities are attributed at bifurcations, whose values are indicated on the edges. These probability values are selected randomly, with some exceptions. In particular, at those bifurcations where flow is distributed as 0.1 - 0.9, values have been specifically imposed by us, so as to direct more water volume towards outlet 2 and 3, differently from the previous case.

The simulation results are shown in figures 3.19 and 3.20. These must be compared respectively to 3.17 and 3.18, since the input distributions we use (the dashed black lines) are the same as the above paragraph: two deltas for the first

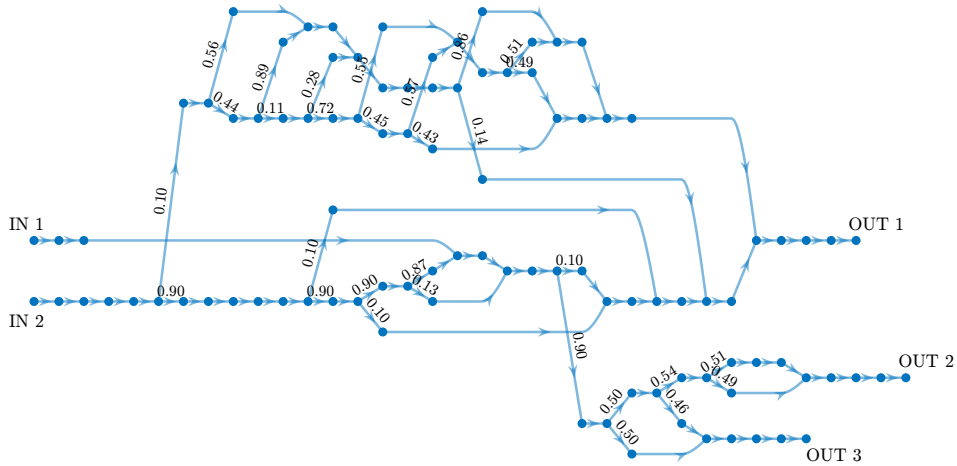


Figure 3.16: Same graph with 2 inlets and 3 outlets as in fig. 3.15. Mean waiting times are still supposed equal to 1 in all edges, but we introduce the hypothesis of non-symmetric bifurcations. The non-trivial probability values at bifurcations are shown here; some of them have been randomly chosen, some others are imposed specifically to redirect the flow towards outlet 2 and 3.

case and two different gammas for the second. The injected volume is always normalised to 1.

In all figures we see that the red curve corresponding to outlet 3 is now above the blue curve of outlet 1. This means that we have indeed been able to redirect the volume away from outlet 1. Percentages have dropped from 50% to 10% as far as concerns inlet 1 and from 94% to 34% for the second inlet. Consequently the volume fractions reaching outlet 2 and 3 are also much higher.

Comparing 3.19c to 3.17c, we notice the presence of two peaks which were absent earlier. We can explain this by looking again at the graph in figure 3.16. The paths going to outlet 2 or 3 can have very different lengths depending on whether they start at inlet 1 or 2. This is reflected in a consistent shift of the peak of the red and green IUHs in fig. 3.19a with respect to fig. 3.19b. In the previous set of simulations the two distinct peaks could not be detected because of the very low volume fractions reaching outlet 2 and 3.

Again if we inject two gammas instead (fig. 3.20) the area values and the features we have pointed out are the same. The curves shape obviously changes, since these are obtained convolving gamma distributions with the very narrow IUHs of fig. 3.19.

What we intend to show with these numerical simulations, is that the bifurcation probability values can have a strong impact on how the volume is distributed among different outlets.

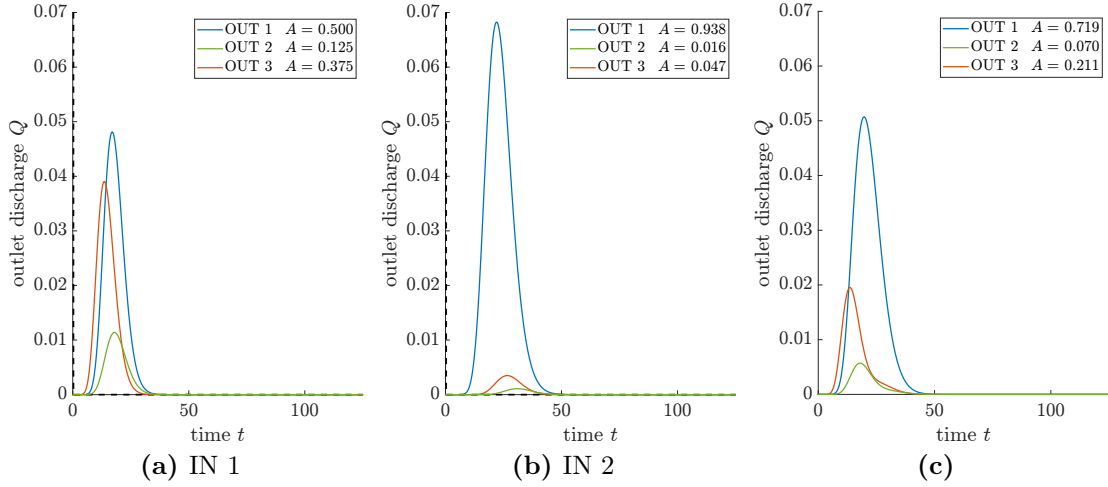


Figure 3.17: Travel time distributions at the outlets of the network in figure 3.15, in the case of waiting times equal to 1 in each edge and symmetric bifurcations, supposing delta distributions in input (the dashed black lines). Within the legend we report the colors corresponding to each outlet and the values of the area under each curve. (a) Discharges considering the input from inlet 1 only. (b) Discharges considering the input from inlet 2 only. (c) Total discharges considering both inlets.

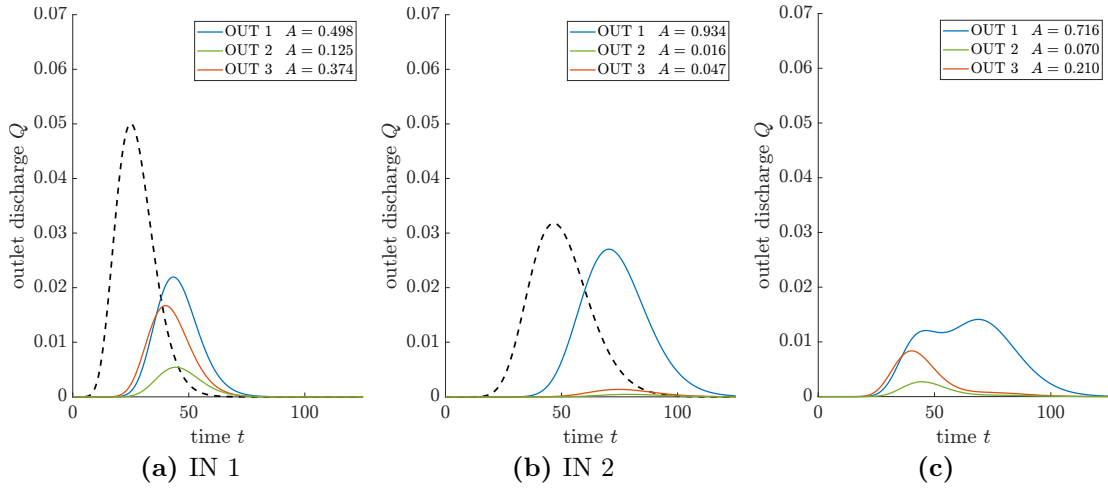


Figure 3.18: Travel time distributions at the outlets of the network in figure 3.15, in the case of waiting times equal to 1 in each edge and symmetric bifurcations, supposing gamma distributions in input (the dashed black lines). Within the legend we report the colors corresponding to each outlet and the values of the area under each curve. (a) Discharges considering the input from inlet 1 only. (b) Discharges considering the input from inlet 2 only. (c) Total discharges considering both inlets.

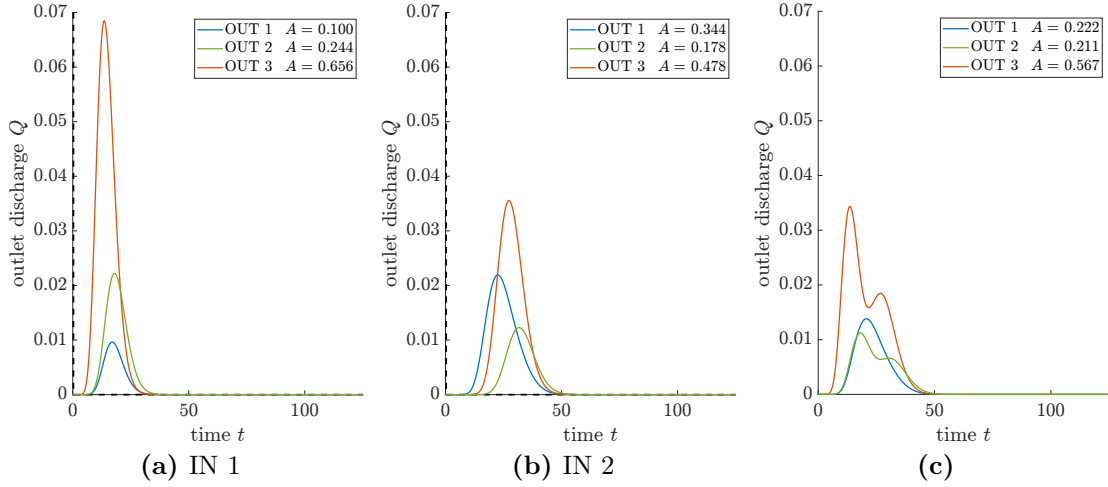


Figure 3.19: Travel time distributions at the outlets of the network in figure 3.15, in the case of waiting times equal to 1 in each edge and non-symmetric bifurcations, supposing delta distributions in input (the dashed black lines). Within the legend we report the colors corresponding to each outlet and the values of the area under each curve. (a) Discharges considering the input from inlet 1 only. (b) Discharges considering the input from inlet 2 only. (c) Total discharges considering both inlets.

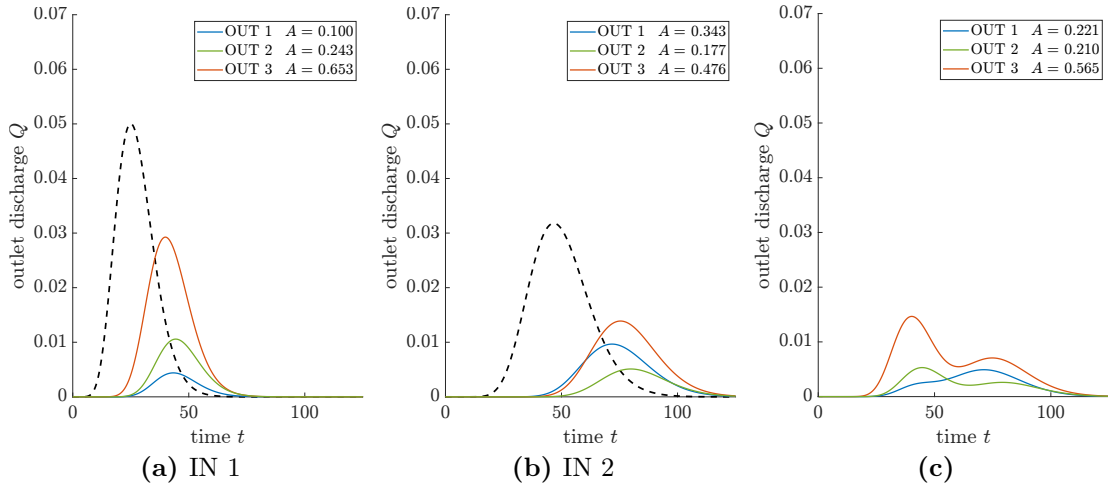


Figure 3.20: Travel time distributions at the outlets of the network in figure 3.15, in the case of waiting times equal to 1 in each edge and non-symmetric bifurcations, supposing gamma distributions in input (the dashed black lines). Within the legend we report the colors corresponding to each outlet and the values of the area under each curve. (a) Discharges considering the input from inlet 1 only. (b) Discharges considering the input from inlet 2 only. (c) Total discharges considering both inlets.

Conclusions

The intent of our thesis work was to investigate solute transport processes in river networks. We decided to focus on dispersion mechanisms and in particular geomorphological dispersion. This term indicates a class of dispersive phenomena related only to the network structure and properties. In addition, we identified the object of our study with braided rivers, a class of fluvial network characterized by the presence of multiple channels, of different size that bifurcate and merge forming an extremely complex and fascinating network morphology. For this reason, we expected the geomorphological contribution to take an extremely important part in determining dispersion values for rivers with a braided pattern.

For this purpose, we developed a mathematical model to compute the discharge rate distribution at a river outlet, given the network properties and the injected distribution at the inlet. Our model is based on the original GIUH theory approach. A quite uncommon graph-method was used to enclose the river geometry within a matrix form and to allow MATLAB implementation.

Finally we performed some numerical simulations on small networks, which gave some interesting qualitative results. We used graphs both built ad-hoc and extracted from a network representation of Stream Borbera.

To start with, our simulations confirmed the theoretical explanation of how the number of available paths from inlet to outlet is directly related to dispersion. In particular a higher number of paths with a wide range of possible path lengths leads to higher spread in travel time distributions. Then we examined the influence on outlet discharges of some network parameters such as the branches length and the probability values assigned at bifurcations. Surprisingly we found that the role of the graph structure seems to prevail on any parameter value. This result has powerful consequences in the fact that, when studying solute transport, events at scale of the entire network are more important than those at the individual channel scale. Therefore one might avoid focusing so much on determining the properties of each branch and bifurcation, which can be extremely laborious. In the last set of simulations we focused on the case of multiple inlets and outlets. This has been done to show how to combine different functions from different input to contribute to the several outlet discharges.

To conclude, we think that this work opens the door to interesting generalizations of the renowned and well-respected GIUH theory. Furthermore it supports and encourages the application of graph theory to the study of river networks. In the end, it gives some meaningful suggestions on how to rethink and simplify the study of transport processes in fluvial networks.

Bibliography

- Alabyan A. M. and Chalov R. S. (1998). «Types of river channel patterns and their natural controls». In: *Earth Surface Processes and Landforms*.
- Ashmore P. (1991). «How Do Gravel-Bed Rivers Braid?» In: *Geography Publications*.
- Ashworth P. J. and Lewin J. (2012). «How do big rivers come to be different?» In: *Earth-Science Reviews*.
- Botter G., Bertuzzo E., and Rinaldo A. (2011). «Catchment residence and travel time distributions: The master equation». In: *Geophysical Research Letters*.
- Botter G. and Rinaldo A. (2003). «Scale effect on geomorphologic and kinematic dispersion». In: *Water Resources Research*.
- Bouchez J. et al. (2010). «Turbulent mixing in the Amazon River: The isotopic memory of confluences». In: *Earth and Planetary Science Letters*.
- Connor-Streich G. (2019). «Graph theoretical analysis of braided rivers». PhD thesis. Queen Mary University of London.
- Connor-Streich G., Henshaw A. J., Brasington J., Bertoldi W., and G. L. Harvey (2018). «Let's get connected: A new graph theory-based approach and toolbox for understanding braided river morphodynamics». In: *WIREs Water*.
- De Bartolo S. et al. (2022). «Scaling behaviour of braided active channels: a Taylor's power law approach». In: *The European Physics Journal Plus*.
- Deng Z.-Q. and Jung H. S. (2009). «Variable residence time-based model for solute transport in streams». In: *Water Resources Research*.
- Deng Z.-Q., Jung H.-S., and Ghimire B. (2010). «Effect of channel size on solute residence time distributions in rivers». In: *Advances in Water Resources*.
- Di Lazzaro M., Zarlenga A., and Volpi E. (2015). «Hydrological effects of within-catchment heterogeneity of drainage density». In: *Advances in Water Resources*.

- Di Lazzaro M., Zarlenga A., and Volpi E. (2016). «Understanding the relative role of dispersion mechanisms across basin scales». In: *Water Resources Research*.
- Gleyzer A., Denisyuk M., Rimmer A., and Salingar Y. (2004). «A fast recursive GIS algorithm for computing Strahler stream order in braided and nonbraided networks». In: *Journal of the American Water Resources Association*.
- Gooseff M. N., Hall R. O., and Tank J- L. (2007). «Relating transient storage to channel complexity in streams of varying land use in Jackson Hole, Wyoming». In: *Water Resources Research*.
- Gooseff M. N., LaNier J., Haggerty R., and Kokkeler K. (2005). «Determining in-channel (dead zone) transient storage by comparing solute transport in a bedrock channel–alluvial channel sequence, Oregon». In: *Water Resources Research*.
- Gooseff M. N., Wondzell S. M., Haggerty R., and Anderson J. (2003). «Comparing transient storage modeling and residence time distribution (RTD) analysis in geomorphically varied reaches in the Lookout Creek basin, Oregon, USA». In: *Advances in Water Resources*.
- Gupta V. K., Waymire E., and Wang C. T. (1980). «A Representation of an Instantaneous Unit Hydrograph from Geomorphology». In: *Water Resources Research*.
- Haggerty R., Wondzell S. M., and Johnson M. A. (2002). «Power-law residence time distribution in the hyporheic zone of a 2nd-order mountain stream». In: *Geophysical Research Letters*.
- Heckmann T., Schwanghart W., and Phillips J. D. (2015). «Graph theory — Recent developments of its application in geomorphology». In: *Geomorphology*.
- Hiatt M, Sonke W., and Addink E. A. (2019). «Geometry and Topology of Estuary and Braided River Channel Networks Automatically Extracted From Topographic Data». In: *JGR Earth Surface*.
- Howard R. A. (1971). *Dynamic Probabilistic Systems*. Vol. II: Semi-Markov and Decision Processes. John Wiley.
- Kleinmans M. G. (2010). «Sorting out river channel patterns». In: *Progress in Physical Geography-Earth and Environment*.
- Malverti L., Lajeunesse E., and Metivier F. (2008). «Small is beautiful: Upscaling from microscale laminar to natural turbulent rivers». In: *Journal of Geophysical Research*.

- Marra W. A., Kleinhans M. G., and Addink E. A. (2013). «Network concepts to describe channel importance and change in multichannel systems: test results for the Jamuna River, Bangladesh». In: *Earth Surface Processes and Landforms*.
- Murray A. B. and Paola C. (1994). «A cellular model of braided rivers». In: *Nature*.
- Newman M. (2010). *Networks: An Introduction*. Oxford University Press.
- Phillips J. D., Schwanghart W., and Heckmann T. (2015). «Graph theory in the geosciences». In: *Earth-Science Reviews*.
- Rigon R., Bancheri M., Formetta G., and de Lavenne A. (2016). «The geomorphological unit hydrograph from a historical-critical perspective». In: *Earth Surface Processes and Landforms*.
- Rigon R., Bancheri M., and Green T. R. (2016). «Age-ranked hydrological budgets and a travel time description of catchment hydrology». In: *Hydrology and Earth System Sciences*.
- Rinaldi M., Gurnell A. M., Tánago Gonález del, Bussettini M., and Hendriks D. (2016). «Classification of river morphology and hydrology to support management and restoration». In: *Aquatic Sciences*.
- Rinaldo A., Marani A., and Rigon R. (1991). «Geomorphological Dispersion». In: *Water Resources Research*.
- Rinaldo A. and Rodriguez-Iturbe I. (1996). «Geomorphological theory of the hydrological response». In: *Hydrological Processes*.
- Rodriguez-Iturbe I. and Valdés J. B. (1979). «The Geomorphologic Structure of Hydrologic Response». In: *Water Resources Research*.
- Rosgen D. L. (1994). «A classification of natural rivers». In: *Catena*.
- Runkel R. L. and Bencala K. E. (1995). «Transport of reacting solutes in rivers and streams». In: *Environmental Hydrology*. Ed. by Vijay P. Singh. Springer Netherlands.
- Saco P. M. and Kumar P. (2002). «Kinematic dispersion in stream networks - 1. Coupling hydraulic and network geometry». In: *Water Resources Research*.
- Schuurman F. (2015). «Bar and channel evolution in meandering and braiding rivers using physics-based modeling». PhD thesis. Utrecht University.
- Williams R. D., Brasington J., and Hicks D. M. (2016). «Numerical Modelling of Braided River Morphodynamics: Review and Future Challenges». In: *Geography Compass*.